



MIT Open Access Articles

Defect detection in FRP-bonded structural system via phase-based motion magnification technique

The MIT Faculty has made this article openly available. **Please share** how this access benefits you. Your story matters.

Citation	Qiu, Qiwen and Lau, Denvi. 2018. "Defect detection in FRP-bonded structural system via phase-based motion magnification technique." Structural Control and Health Monitoring, 25 (12).
As Published	http://dx.doi.org/10.1002/stc.2259
Publisher	Wiley
Version	Author's final manuscript
Citable link	https://hdl.handle.net/1721.1/140892
Terms of Use	Article is made available in accordance with the publisher's policy and may be subject to US copyright law. Please refer to the publisher's site for terms of use.

Lau Denvi (Orcid ID: 0000-0003-3454-3938)

**Defect detection in FRP-bonded structural system via phase-based motion
magnification technique**

Qiuwen Qiu¹ and Denvi Lau^{1,2,*,\dagger}

¹ *Department of Architecture and Civil Engineering, City University of Hong Kong,
Hong Kong, China.*

² *Department of Civil and Environmental Engineering, Massachusetts Institute of
Technology, Cambridge, MA 02139, USA.*

* Correspondence to: Denvi Lau

\dagger E-mail: denvi@mit.edu

SUMMARY

Fiber reinforced polymer (FRP) bonded structural systems have been increasingly used in the field of civil infrastructure. Despite the outstanding advances in the applications of these structures, the interfacial defect between FRP composite and basis material occur frequently during the designed service life. This type of defect can severely reduce the system integrity, which requires appropriate methods for defect detection in order to control the structural health state. This paper presents a

This is the author manuscript accepted for publication and has undergone full peer review but has not been through the copyediting, typesetting, pagination and proofreading process, which may lead to differences between this version and the [Version of Record](#). Please cite this article as doi: [10.1002/stc.2259](https://doi.org/10.1002/stc.2259)

novel approach of using phase-based motion magnification technique for detection of interfacial defect in FRP-bonded structural system. The research demonstrates that this video processing technique can effectively amplify the small surface motion at the defect location of FRP-bonded panel exposed to an air blow. The defect location and shape can be distinguished from the surrounding intact region, given that the two important parameters of bandpass frequency range and motion amplification factor are appropriately selected. Based on the research findings, a suitable defect detection scheme towards the FRP-bonded structural systems via this computational technique is established. The offered methodology does not require sensor installation and wiring, which enables an inexpensive and practical way for structural assessment.

KEY WORDS: Computational technique; Defect detection; Fiber reinforced polymer bonded structural system; System identification; Structural health assessment

1. INTRODUCTION

Fiber reinforced polymer (FRP) material features its high specific stiffness and strength, good fatigue performance and damage tolerance, which can effectively improve the flexural and shear capacity of engineering structures [1-4]. In

construction and building technology, this composite has been widely used to strengthen the existing deficient concrete structures. Also, it can promote the wide utilization of wood materials in buildings due to the following two important benefits: (a) enhancing the load-carrying capacity of wood elements (e.g. lumber, veneers, flakes, and strands) by bonding FRP and (b) saving the construction energy as wood is a renewable and green building material in comparison to cement, concrete and steel [2, 5-8]. Nevertheless, FRP-bonded structural system suffers from interface deterioration and defect initiation due to outside instant impact or environmental attacks. The deterioration of FRP-bonded wood structure can be more serious since the wood component is susceptible to chemical degradation, fungal infection, and entry of pathogens and insects [9-13]. Hence, the interfacial defect between the FRP and the substrate frequently occur. In this circumstance, the strengthening efficiency by using FRP composite is limited. With the increasing use of FRP-bonded structural system in the field of civil engineering infrastructure, suitable and accurate detection to the bonding condition between the FRP and the basis material is important for maintaining the structural performance.

Currently, many remarkable technologies have been investigated or employed in defect detection of FRP-bonded composite beams, plates and columns. Most of the methods are relied on detecting the mechanical wave propagated through the

composite material or electromagnetic signal reflected from the target [14]. Mechanical wave based techniques (*e.g.* acoustic emission technique [15, 16], photophone-based approach [17], and ultrasonic technique [18]) have received considerable attentions for damage evaluation of bonded structural system. Besides, electromagnetic wave based techniques (*e.g.* radar technology [19, 20], infrared thermography [21, 22], impedance measurement [23], and laser reflection technique [24, 25]) have been used to evaluate deterioration of FRP-bonded structural system with great success. More recently, acoustic-laser technique that combines the use of mechanical wave (white noise) and electromagnetic wave (laser) has been developed to detect the presence of defect in FRP-bonded plates or columns [25-28]. Although the above methods have the ability to identify the defect in composite systems, the direct structural response cannot be obtained as the received signals are required to be interpreted. Besides, more sophisticated equipment and devices, more specialized data post-treatment and probably much higher costs are demanded in these techniques [29]. Moreover, noise component is often included in the received signals, which affects the inspection accuracy. In order to detect the defect in FRP-bonded structural system in a more direct and reliable manner, defect visualization becomes interesting and valuable.

As to interfacial defect in FRP-bonded structural system, the defect visualization can be more probably realized. With the presence of near surface defect in FRP-bonded structural system, the surface vibration behaviour at the defect region varies from the intact region when an external mechanical excitation is applied [30]. Among the mechanical excitation ways like using air suction cup [31] and direct mechanical loading [32], the utilization of instant air blow is regarded to be non-invasive, non-contact, convenient and efficient for initiating the structural vibration. When this air blow is applied, the FRP surface vibration at the defect region takes place with its natural frequency (usually from hundreds to thousands). However, such rapid vibration phenomenon is hard to be well observed by naked eye. Generally, this issue can be addressed by adopting the high speed camera which can record the fast motion and play the medium back in slow-motion manner. Another issue is that the vibration is too subtle to be visible due to the high stiffness of FRP plate. With the purpose to solve this problem, video processing methods are encouraged for amplifying the surface motion at the defect region. Thus, the defect location and shape are expected to be visualized from the recorded video. Vision-based technique has been increasingly used in the field of structural health assessment due to its merits of automation, operational convenience, and efficiency [33-36]. During the past few years, phase-based motion magnification technique has been developed to magnify

the interested motion in a video, with the features of low computation cost and good noise handling performance [37-39]. In this technique, the input video is decomposed by complex-valued steerable pyramids and the local phase over time at every spatial scale and orientation of a steerable pyramid is computed. Then, the interested phase component is temporally isolated with a bandpass frequency filter and the bandpassed phase is multiplied by an amplification factor. At the final stage, the magnified phase and the amplitude are reconstructed back into video. Recently, researchers have applied the phase-based motion magnification technique to characterize the vibration behaviour and perform the modal analysis of simple structures such as steel cantilever beam and pipe cross section [40]. Considering the excellent performance of video processing, it is motivated to investigate the use of phase-based motion magnification technique towards the defect visualization for FRP-bonded structural system. Compared to the conventional methods based on receiving and analyzing the mechanical and electromagnetic signals, the phase-based motion magnification technique may allow direct observation of the structural defect from the recorded video since that the vibration phenomenon at the defect region can be amplified and distinguished from the intact region. Besides, in this approach, the setup is convenient and the detection is conducted on observing the processed video showing the whole structural surface instead of point-by-point measurement. This

can significantly improve the efficiency of defect detection for FRP-bonded structural system.

The objective of this study is to develop an innovative defect detection scheme in FRP-bonded structural system via phase-based motion magnification technique. In the experimental work, FRP-bonded wood panel with interfacial defect is fabricated as the representative of FRP-bonded structural system, since this type of structure is increasingly used and will be commonly applied in structural field. The specimen is subjected to instant air blow, which is recorded by a high speed camera. Results of defect visualization in video processed by phase-based motion magnification technique are demonstrated. In addition, the two important factors (*i.e.* bandpass frequency range and motion amplification factor) during the video processing are evaluated to optimize the detection performance. Recommendations of selecting these two parameters for reliable defect detection are provided. Moreover, future development of this methodology in inspection of FRP-bonded structural system is discussed.

2. THEORETICAL SECTION

2.1. Phase-based motion magnification technique

Motion analysis technique from video attracts wide attention in the field of structural engineering. Many researchers in computer vision community have developed algorithms to improve the analysis performance. Calculating the phase gradient of a spatio-temporally bandpass image sequences to obtain the constant phase contours has been studied, which demonstrates an excellent approximation to the real motion [41, 42]. However, this method requires much optical flow computation. More recently, linear Eulerian video processing has been investigated and used for dampening temporal aliasing of motion in videos and for exhibiting subtle color variations and small motions [43, 44]. This video processing technique relies on a first-order Taylor approximation to independently process the time series of color values at each pixel, avoiding the need for costly flow computation. Nevertheless, linear Eulerian video processing allows merely small magnification levels at high frequency of spatial domain due to the reliance of first-order Taylor expression [38]. In addition, this technique can significantly amplify noise (*e.g.* ghosting flows) when the amplification factor is increased [45]. To address the above limitations, another phase-based magnification approach for motion processing has been developed in past several years, which computes the local phase variations for measuring motion in video by Fourier shift theorem. The appeal of phase-based motion magnification is that it avoids explicit optical flow computation and it is significantly less sensitive to noise

[37-39]. Generally, in this technique, the input image sequence (considering the case of a one dimensional image intensity I) is decomposed into a multiscale stack by means of Gabor wavelets which are sinusoidal functions modulated by a Gaussian envelope as expressed by Equation (1).

$$g(x) = e^{\frac{-x^2}{2\sigma^2}} \exp(-iwx) \quad (1)$$

where x is the independent spatial variable of the Gabor wavelet, w is the frequency of the complex sinusoid, and σ is the standard deviation of the Gaussian envelope, modulating the sinusoidal function $\exp(-iwx)$. Equation (1) has real and imaginary parts [46, 47]:

$$g(x) = A(x) + iB(x) \quad (2)$$

$$A(x) = e^{\frac{-x^2}{2\sigma^2}} \cos(2\pi w_0 x) \quad (3)$$

$$B(x) = e^{\frac{-x^2}{2\sigma^2}} \sin(2\pi w_0 x) \quad (4)$$

When the one dimensional intensity image $I(x, t)$ experiences a finite value of motion δ_x in the spatial domain, the new image is resulted and expressed by $I(x + \delta_x, t)$ [48]. During the image decomposition, the first frame of the one dimensional image and the second frame image after the motion δ_x are convoluted with the complex Gabor filter $g(x)$.

$$\tilde{I} = I * g(x) \quad (5)$$

where \tilde{I} refers to image intensity after convolution by Gabor filter. As a result, the convoluted image intensity at two time frames will be mapped to a complex valued domain called $\tilde{I}_1(u)$ and $\tilde{I}_2(u)$, respectively, as expressed by Equations (6) and (7).

$$\tilde{I}_1(u) = \int_{-\infty}^{+\infty} I(x-u) e^{\frac{-x^2}{2\sigma^2}} e^{-i2\pi x} dx \quad (6)$$

$$\tilde{I}_2(u) = \int_{-\infty}^{+\infty} I(x+\delta_x-u) e^{\frac{-x^2}{2\sigma^2}} e^{-i2\pi x} dx \quad (7)$$

where $\tilde{I}_1(u)$ refers to the convoluted image intensity at frame 1, and $\tilde{I}_2(u)$ refers to the convoluted image intensity at frame 2. By converting the independent variable $x+\delta_x$ into β in Equation (7), the phase-based motion presentation for one dimensional intensity image can be obtained as Equation (8).

$$\tilde{I}_2(u) = \int_{-\infty}^{+\infty} I(\beta-u) e^{\frac{-(\beta-\delta_x)^2}{2\sigma^2}} e^{-i2\pi(\beta-\delta_x)} d\beta \quad (8)$$

In the above equations, the phase values in the first and second frame of the one dimensional image intensity can be denoted as φ_1 and φ_2 expressed by Equations (9) and (10) [48].

$$\varphi_1 = \arg[\tilde{I}_1(u)] = 2\pi\beta \quad (9)$$

$$\varphi_2 = \arg[\tilde{I}_2(u)] = 2\pi(\beta - \delta_x) \quad (10)$$

The phase change $\Delta\varphi$ between the two consecutive frames can be further derived as:

$$\Delta\varphi = \varphi_1 - \varphi_2 = 2\pi\delta_x \quad (11)$$

When amplifying $\Delta\varphi$ by a factor α , the phase change becomes $\alpha\Delta\varphi$. Using this value to shift the Fourier coefficients of $I(x, t)$ can yield $I(x + (1 + \alpha)\delta_x, t)$ [38]. The above principle of phase-based motion technique can be extended to two dimensional spatial functions or images. However, in most real cases, the motion in video cannot be regarded as the global translations of a frame over time but local and complicated spatially-varying movement. Hence, the complex steerable pyramid (complex, overcomplete linear transform) is adopted in the phase-based motion technique to break the image into local sinusoids [45]. The steerable pyramid is built by applying the Gabor filters to decompose the discrete Fourier transform of an image I into different spatial frequency sub-bands simultaneously localized in position, spatial scale and orientation. Then, the local phase at every spatial scale and orientation of the steerable pyramid is computed. After that, the phases are temporally filtered to isolate the interested motion related to the natural frequency of surface vibration in structure. And then, the bandpass phase in the corresponding frequency range is amplified by a factor. Finally, this magnified phase and the amplitude of the original image is reconstructed back so that the magnified video is rendered. The phase-based motion magnification method has the advantages over the previous Eulerian magnification method in terms of two important perspectives: larger magnification achievement and better noise performance. This method modifies

phases instead of amplitudes, without the increase in level of spatial noise. In this research, the phase-based motion magnification was adopted to enlarge the surface vibration at defect region in the FRP-bonded structural system.

2.2. Motion amplification factor

From the literature about the phase-based motion magnification [38], the intensity of phase after magnification can be attenuated when Gaussian window of the Gabor filters are applied. Increasing the motion amplification factor may reach the limit where we cannot move the feature because of the limited spatial support of each pyramid filter. Therefore, we need to set the maximum amplification factor such that the amplified motion approximates well the true signal. According to the suggestion of the above literature, the one standard deviation of the Gaussian window is used as the bound, which is described by Equation (12).

$$\alpha\delta(t) < \sigma \quad (12)$$

Where α is the amplification factor, $\delta(t)$ the phase difference, and σ is the standard deviation of Gaussian window. For the half octave pyramid, there are approximately two periods of the sinusoid under the Gaussian envelope of the wavelet. That is:

$$4\sigma \approx \frac{2}{w_o} \quad (13)$$

Where w_o is the frequency of the selected filter. This gives Equation (14).

$$\alpha\delta(t) < \frac{1}{2w_0} \quad (14)$$

Exceeding the above limit can cause flaws or blur, as the Gaussian function used for this approach breaks up. Hence, the motion amplification factor is investigated in this study to better apply the video processing technique for visualizing the defect in FRP-bonded structural system.

2.3. Bandpass frequency range

In addition to the motion amplification factor, selecting the appropriate bandpass frequency range is also needed to be concerned. In phase-based motion magnification technique, the phases are temporally bandpass filtered within a certain frequency range that approximates the motion frequency of target. With respect to the FRP-bonded structural system with interfacial defect, the FRP surface at the defect region starts to vibrate at its natural frequency after subjecting to an instant air blow. Thus, selecting the appropriate bandpass frequency range that covers the natural frequency of surface vibration at the defect region is critical for achieving satisfactory signal-to-noise level. According to the theory of plate vibration [49-51], the natural frequency f is determined by material properties of FRP and defect area, as expressed by Equations (15), (16) and (17).

$$D\nabla^4 w + \rho h \frac{\partial^2 w}{\partial t^2} = 0 \quad (15)$$

$$D = \frac{Eh^3}{[12(1 - \nu^2)]} \quad (16)$$

$$f = \frac{\lambda}{a^2} \sqrt{\frac{D}{\rho h}} \quad (17)$$

where E refers to Young's modulus (GPa), h refers to thickness (mm), ν refers to Poisson's ratio of FRP composite, $w = w(x, y, t)$, representing the transverse displacement of the plate as a function of spatial variables x , y , and time t , ρ refers to density of FRP plate, λ refers to the frequency coefficient, which is 35.99 for square plate with four clamped sides. In this paper, importance of selecting the appropriate bandpass frequency range in phase-based motion magnification technique for defect detection of FRP-bonded structural system is demonstrated. Additionally, recommendations of how to choose a good bandpass frequency range are provided.

3. EXPERIMENTAL WORK

3.1. Specimen details

In this study, carbon fiber reinforced polymer (CFRP) bonded wood panel was produced as the representative of FRP-bonded structural system. CFRP sheet with thickness of 0.167 mm, Poisson's ratio of 0.33, density of 1800 Kg/m³ and Young's modulus of 50 GPa was pre-fabricated in the laboratory and then bonded on the top surface of substrate (*i.e.* wood). Two types of defects, namely, internal air block and

interfacial air gap, were respectively made in the CFRP-bonded wood system. On the one hand, to fabricate the FRP-bonded wood panel with internal air block, two wood plates were prepared with thicknesses of 20 mm and 40 mm respectively. A square air hole was made in the central position of wood layer with 20 mm thick. Then, the two wood blocks were bonded by using epoxy resin so that the wood substrate with a surface air hole was fabricated. Afterwards, the pre-fabricated FRP sheet was bonded to the top surface of wood substrate by epoxy resin. As a result, the internal air block with 20 mm thick underneath the FRP layer was produced to represent the bonding defect caused by wood damage or deterioration. On the other hand, to produce the interfacial air gap in FRP-bonded wood panel, a wood plate with 40 mm thickness was prepared as the substrate. Epoxy resin was applied on the surface of this wood plate except the defect zone. Then, the FRP sheet is bonded to the top surface of epoxy layer so that the interfacial air gap was left underneath the FRP layer. The interfacial defect depth equals to the thickness of epoxy layer applied on the wood surface. The two types of defect were evaluated by our proposed method, with the purpose to examine whether or not the depth of the superficial defect can influence the effectiveness of defect identification. Besides the type of defect, the number and dimension of defect were varied in CFRP-bonded

wood panel with interfacial air gap. Figure 1 shows the schematic diagram and photograph of the specimens with different defect cases in this research work.

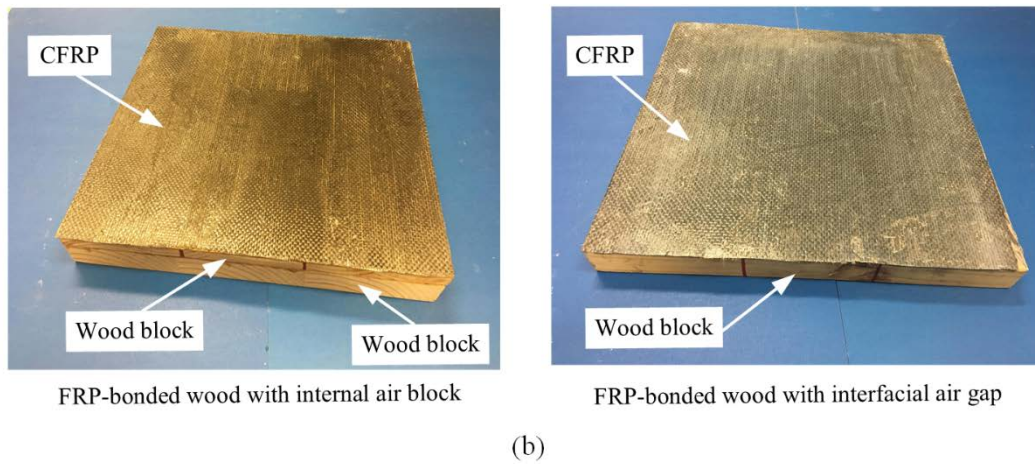
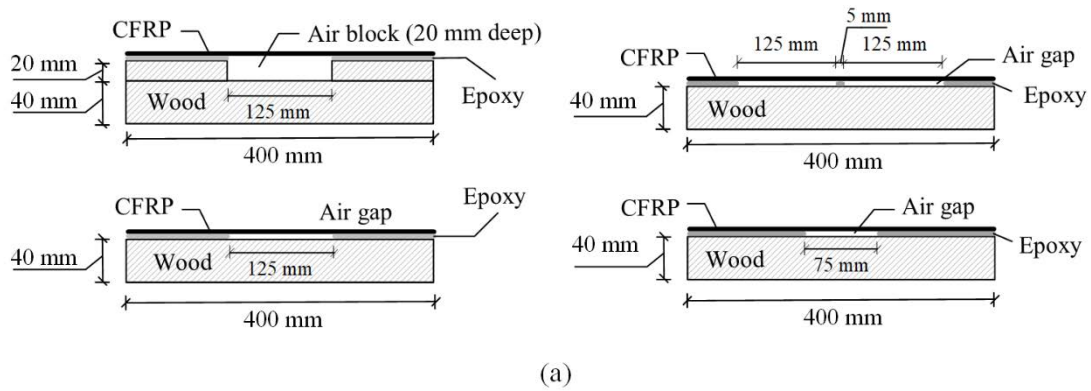
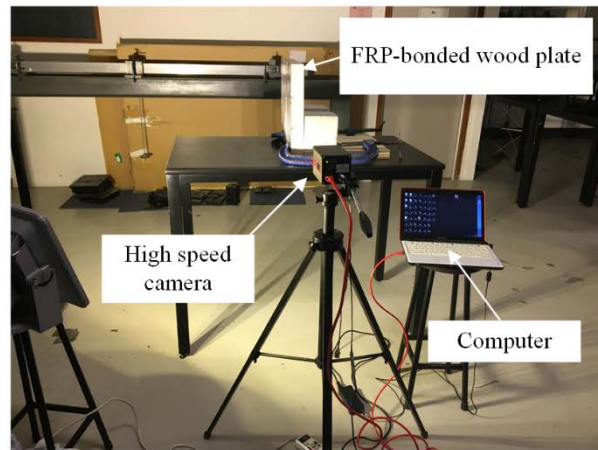
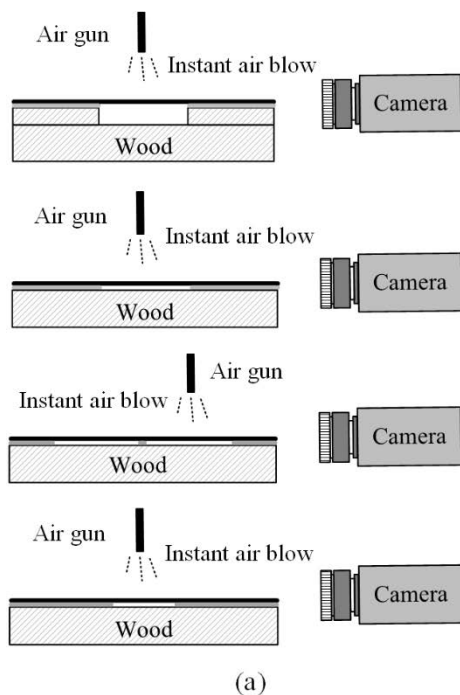


Figure 1. Specimen details of FRP-bonded structural systems under evaluation by phase-based motion magnification: (a) schematic diagram of FRP-bonded wood panel with internal air block and FRP-bonded wood panel with interfacial air gap, (b) photograph of FRP-bonded wood panels with two defect cases.

3.2. Experimental setup

The setup of experimental work was consisted of the air blow producer, the high speed camera, and the tested specimen. Figures 2 depict the schematic diagram and photograph of experimental setup. An instant air blow was applied towards the FRP-bonded structural panel to initiate the surface vibration of the specimen. The instant air blow was produced by an air gun machine from the laboratory. The incident angle of air blow excitation was 0° . The side view of specimen and its vibration behaviour was recorded by a high speed camera. The resolution of the camera was 800×600 , and the frame rate was 1000 frames per second. In addition, the output video frame rate was one per second for the sake of better observation of vibration behaviour.



(b)

Figure 2. Experimental details of defect detection in FRP-bonded structural system by using phase-based motion magnification technique: (a) schematic diagram of experimental setup for detection scheme, and (b) photograph of experimental work.

3.3. Video processing

In order to amplify the surface motion of FRP-bonded structural system under instant air blow, phase-based motion magnification technique was used in this study. Normally, this video processing technique involved in four steps. The first one was using the complex steerable pyramid to decompose the video into a series of amplitude and phase images. In this stage, half-octave bandwidth filters were used in the process of video decomposition. Then, the decomposed phases were bandpass filtered. Due to the 1000 recorded frame rate and the 1 output frame rate, the bandpass frequency range was from 0 to 0.5 Hz according to the Nyquist principle. Since the FRP plate at the defect region vibrates at its natural frequency, the selected bandpass frequency range can have a great influence on the signal-to-noise level in our detection system. Hence, in this research, we compared two bandpass frequency ranges (i.e. 0–0.25 Hz and 0.25–0.50 Hz) to demonstrate the importance of selecting the appropriate bandpass frequency range when applying the phase-based motion magnification into defect detection. In addition to filtered frequency range, the

amplification factor is a critical parameter to be considered. Due to the convolution by Gaussian window of the Gabor filters, the amplitude of shifted phase is attenuated. Increasing the motion amplification factor can result in the deviation from the true signal of movement and may reach the limit where we cannot move the feature because of the limited spatial support of each pyramid filter. Therefore, we need to bound the motion amplification factor during video processing so that the magnified signal is profound while containing little blur. In this study, after frequency filtering, the phase was magnified by a series of factors from 10 to 5000. Finally, the magnified phase and amplitude were reconstructed and the magnified motion video was derived. In this paper, the snapshots of images before and after motion magnification, with different amplification factors and with different bandpass frequency ranges were presented to demonstrate the effectiveness of defect detection with the aid of phase-based motion magnification technique.

4. RESULTS AND DISCUSSION

4.1. Detection performance of phase-based motion magnification technique

Under an adequate air blow, the defect region in FRP-bonded structural system can experience more significant surface displacement than the intact region. Given that the surface of defect region motions at its natural frequency (usually more than

several hundred Hz), the high speed camera is used to record and present the vibration phenomenon so as to make it clearly observable. Figures 3(a) and (b) shows the images of FRP-bonded wood plate at two time frames before applying the motion magnification technique. Based on the observation, no much displacement variation between the defect region and the intact region can be clearly found. Although the defect region in the image is enlarged in Figures 3(a) and (b), the FRP surface movement is still not obvious. In order to get a clear observation of the surface displacement at the defect region, the phase-based motion magnification technique is performed and the magnified result is illustrated in Figures 3(c) and (d). After applying the motion magnification with amplification factor of 100 and filtered frequency range of 0.25–0.50 Hz, we can find out that the surface motion at the defect region is effectively amplified and distinguished from the intact region, as shown in Figures 3(c) and (d). This means that the phase-based motion magnification technique is capable of visualizing the presence of interfacial defect in FRP-bonded structural system shown in the video recorded by high speed camera.

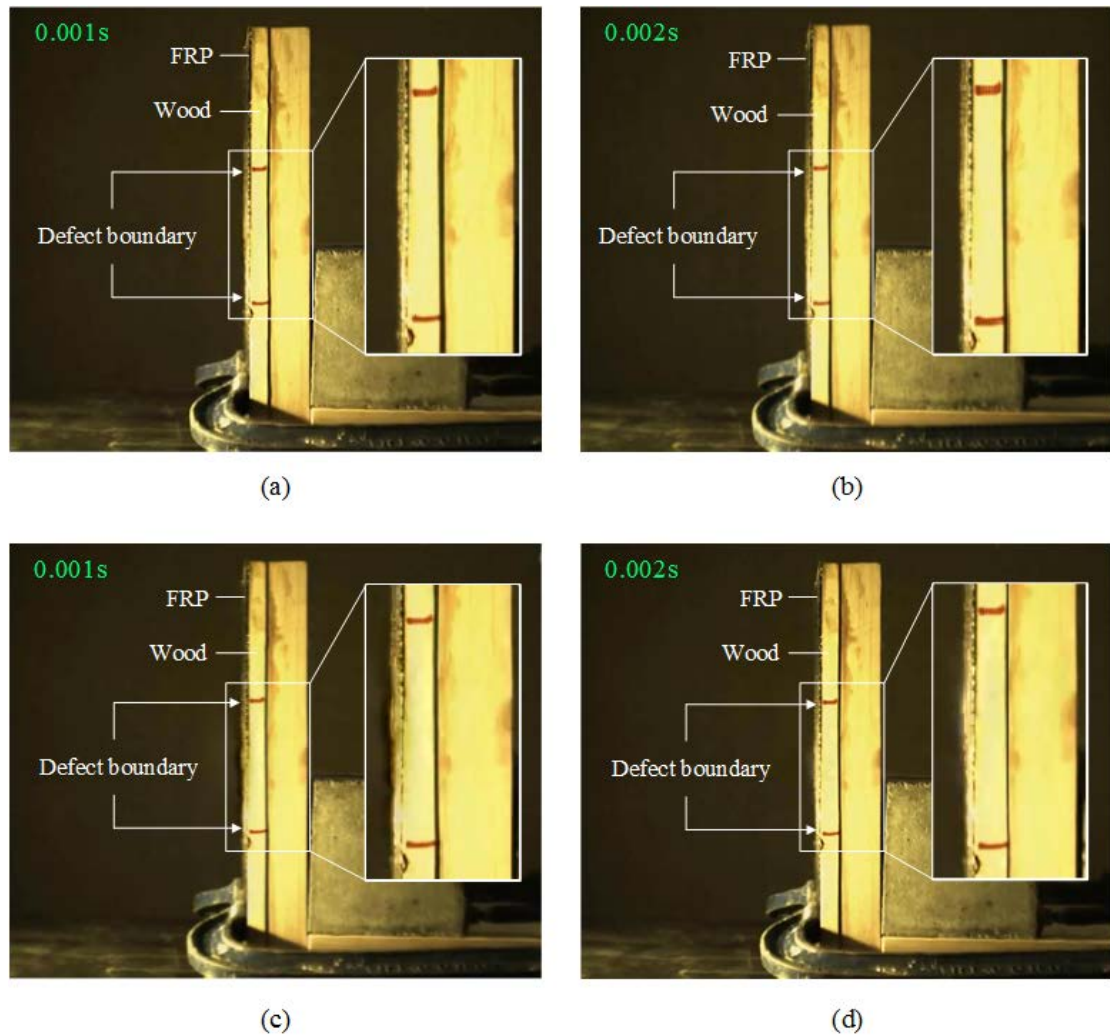


Figure 3. Images of FRP-bonded wood panel with internal air block (125 mm \times 125 mm) under an instant air blow: before motion magnification at (a) 0.001s and (b) 0.002s, and after motion magnification at (c) 0.001s and (d) 0.002s. No significant difference of surface motion between the defect region and the intact region is found during the two periods of time, before the use of motion magnification technique. On the contrary, surface displacement at the defect region is much larger than that of

intact region when motion magnification technique with amplification factor of 100 and bandpass frequency range of 0.25–0.50 Hz is used.

Besides the FRP-bonded wood panel with internal air block, the FRP-bonded wood panel with interfacial air gap is evaluated by the proposed method to examine whether or not the depth of the superficial defect can affect the effectiveness of defect identification. With the identical setting of motion amplification factor and filtered frequency range, the results of motion magnification for FRP-bonded wood panel with interfacial air gap are depicted in Figure 4. A similar surface deflection for both defect cases is found in Figure 3 and Figure 4, indicating that the depth of the superficial defect has little impact on the effectiveness of characterizing the location and shape of structural surface at debonding defect region.

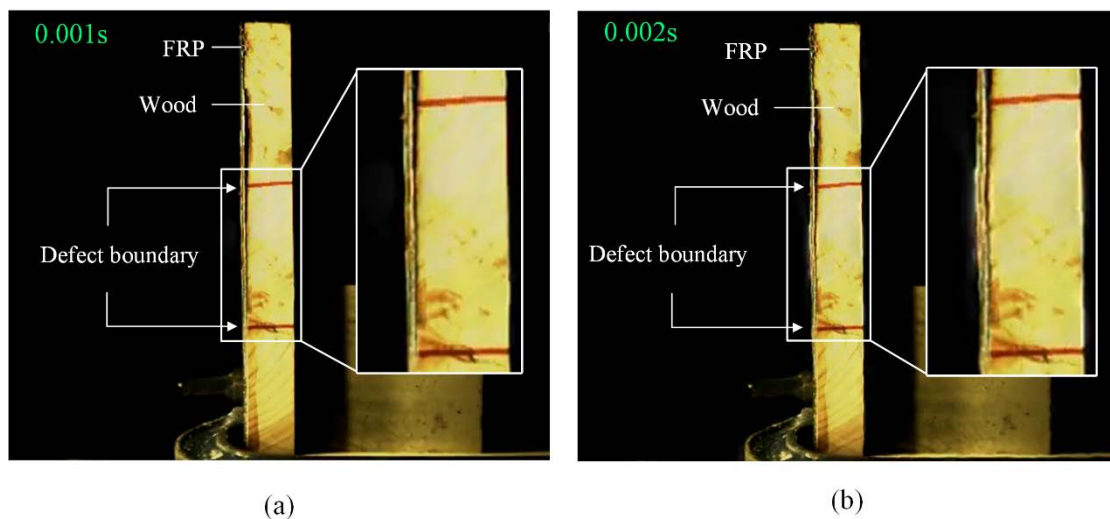


Figure 4. Images after motion magnification for FRP-bonded wood panel with interfacial air gap (125 mm × 125 mm) under an instant air blow: (a) 0.001s and (b) 0.002s. It is found that FRP surface at the defect region with interfacial air gap deforms in a similar pattern to that of defect region with internal air block.

At this stage the experiment is carried out with the focus to measure the specimen with one defect, considering that this research work is fundamental and the basis for using the motion magnification method in defect detection. In the detection of multiple defects in real structure, the video processing technique is used to evaluate each defect region separately with appropriate bandpass frequency range and motion amplification factor. When defects are located closely, the boundary condition for each defect region may be changed. For example, the clamped side of a defect region may be converted to simply supported side. As a result, the mode shape and the natural frequency of each vibrating defect region are modified. In order to consider this issue, we fabricated two interfacial defects that were closely existed in FRP-bonded wood panel, as shown in Figure 1(a). Vibration excitation is applied on one of defect region as described in Figure 2(a). Motion magnification technique is then applied towards this targeted defect region. From Figure 5, it is found that the surface motion near the boundary of defect region seems to be amplified more

remarkably as depicted by the red arrows. Due to the presence of adjacent defect region, the vibration mode shape of the targeted defect region can be varied. In this case, we may consider the FRP plate at this defect region as CCCS plate (three clamped sides and one simply supported side) with frequency coefficient of around 31.8 [52-54]. When optimizing the detection performance, the appropriate bandpass frequency range can be selected according to the deflection shape and natural frequency of this vibrating region. Future work will be carried out to investigate the defect detection with more complicated defect arrangement such as two closely located defects with different sizes.

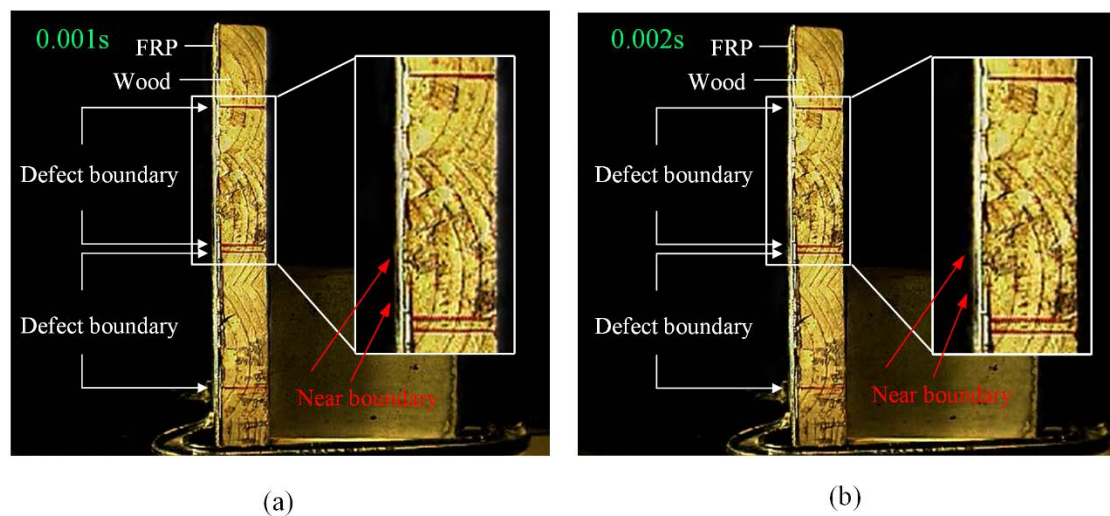


Figure 5. Images after motion magnification for FRP-bonded wood panel with two closely located interfacial air gaps (125 mm \times 125 mm) under an instant air blow: (a) 0.001s and (b) 0.002s. Surface motion near the boundary of defect region is found to

be amplified more remarkably as depicted by the red arrows. Due to the presence of interaction between two defects, the vibration mode shape of the targeted defect region can be changed.

In this study, the high speed camera with the maximum frame rate of 1000 was adopted, indicating that it can analyze the structural vibration with natural frequency up to 500

□Hz (correspondi

criterion. According to the theory of plate vibration [50, 51, 55], the natural frequency f is determined by material properties (*e.g.* Young's modulus) of FRP and defect area A , as expressed by equation (17). Therefore, the smallest detectable dimension A_{min} can be expressed by equation (18) when the natural frequency of 500 Hz is input. Based on the given material properties (*e.g.* Young's modulus of 50 GPa) of CFRP in the detection and the camera used in this study, the smallest detectable dimension A_{min} is estimated as 120 mm × 120 mm approximately.

$$A_{min} = \frac{\lambda}{500} \sqrt{\frac{D}{\rho h}} \quad (18)$$

To clarify this, our high speed camera has also been used to detect the smaller defect with dimension of 75 mm × 75 mm (with natural frequency of 1250 Hz), based on the motion magnification technique. The surface motion of defect region cannot be

effectively observed after the video processing, as shown in Figure 6. In order to perform an effective detection of the smaller defect with the proposed method, a better high speed camera with larger frame rate capacity can be used.

In practical measurement, a high speed camera with larger frame rate is suggested to detect the smaller defect. Table 1 listed the smallest detectable dimension of defect in CFRP-bonded system with the maximum frame rate of commercially available high speed camera. It is also noteworthy that if lower Young's modulus of FRP is used in the composite system, the flexural rigidity of defect region and the corresponding smallest detectable dimension will be reduced, as indicated in equation (18).

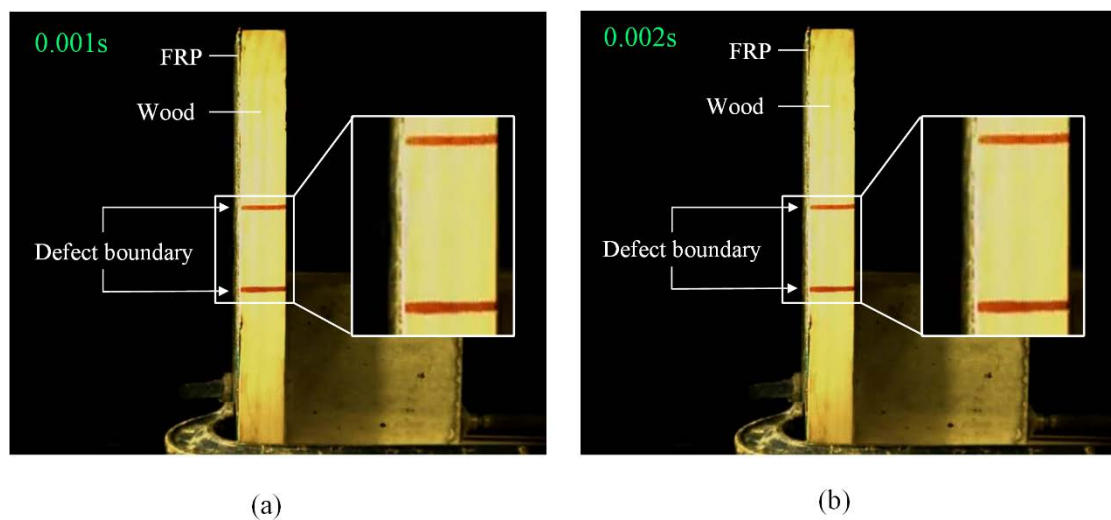


Figure 6. Images after motion magnification for FRP-bonded wood panel with interfacial air gap ($75 \text{ mm} \times 75 \text{ mm}$) under an instant air blow: (a) 0.001s and (b)

0.002s. The surface deformation at defect region cannot be effectively seen after the video processing of motion magnification.

Given that the high speed camera records the side view of FRP-bonded wood structural system, after applying the motion magnification, it is able to quantify the FRP surface displacement value by measuring the movement distance of specimen edge. In order to calculate this FRP surface displacement from the image, the commercial image software Digimizer is adopted. The Digimizer software system uses length of pixels of the image uploaded on the computer, which has been widely adopted by many studies for displacement measurement [56]. In this research, the vibration displacement along with the FRP surface from the bottom to the top is determined. Results are presented in Figure 7. Before motion magnification, the surface displacement is quite small both in defect region and intact region. Also, the variation of surface displacement between defect region and intact region is not considerable. On the contrary, after applying the motion magnification technique, the surface displacement value at the defect region is much larger than that of intact region. The convex shape at the defect region is also clearly found.

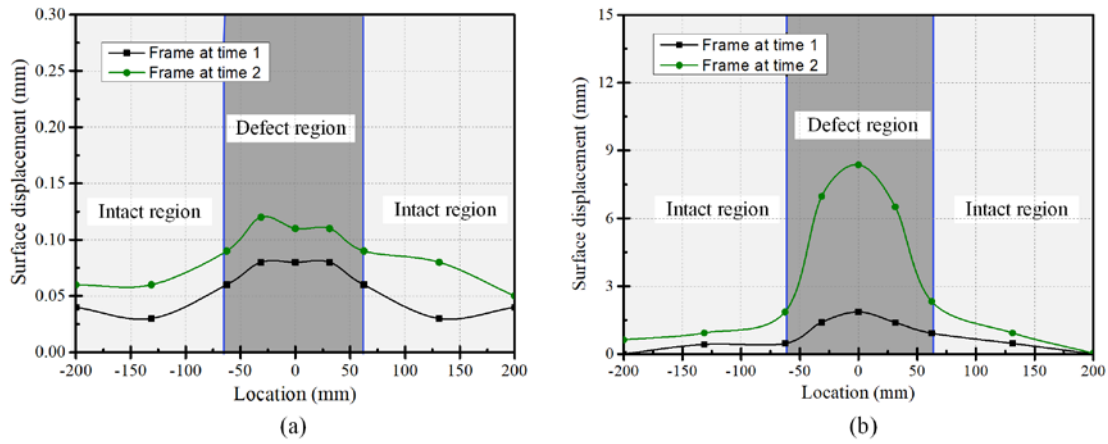


Figure 7. Surface displacement of FRP-bonded wood panel with internal air block both for defect region and intact region: (a) before motion magnification; (b) after motion magnification. Before motion magnification, the variation of surface displacement between the defect region and the intact region is not considerable, while after applying motion magnification the surface displacement at the defect region is much larger than that of intact region.

4.2. Effect of motion amplification factor on defect detection

Figure 8 compares the FRP-bonded wood panel with internal air block with motion amplification factors of 200 and 5000 at two time frames, and bandpass frequency range of 0.25–0.50 Hz. In Figures 8(a) and (b), it can be found that the surface displacement at the defect region can be identified while blurs are rarely found when the motion amplification factor of 200 is used. However, when the motion amplification factor of 5000 is applied, blurs can be clearly observed, as depicted in

Figures 8(c) and (d). This may decline the detection accuracy of defect existed in the structural system. It is indicated that such high motion amplification factor exceeds the limited support of pyramid filter used for video processing. Thus, determining the appropriate amplification factor is essential in the video processing in order to make the magnified motion with high signal-to-noise ratio.

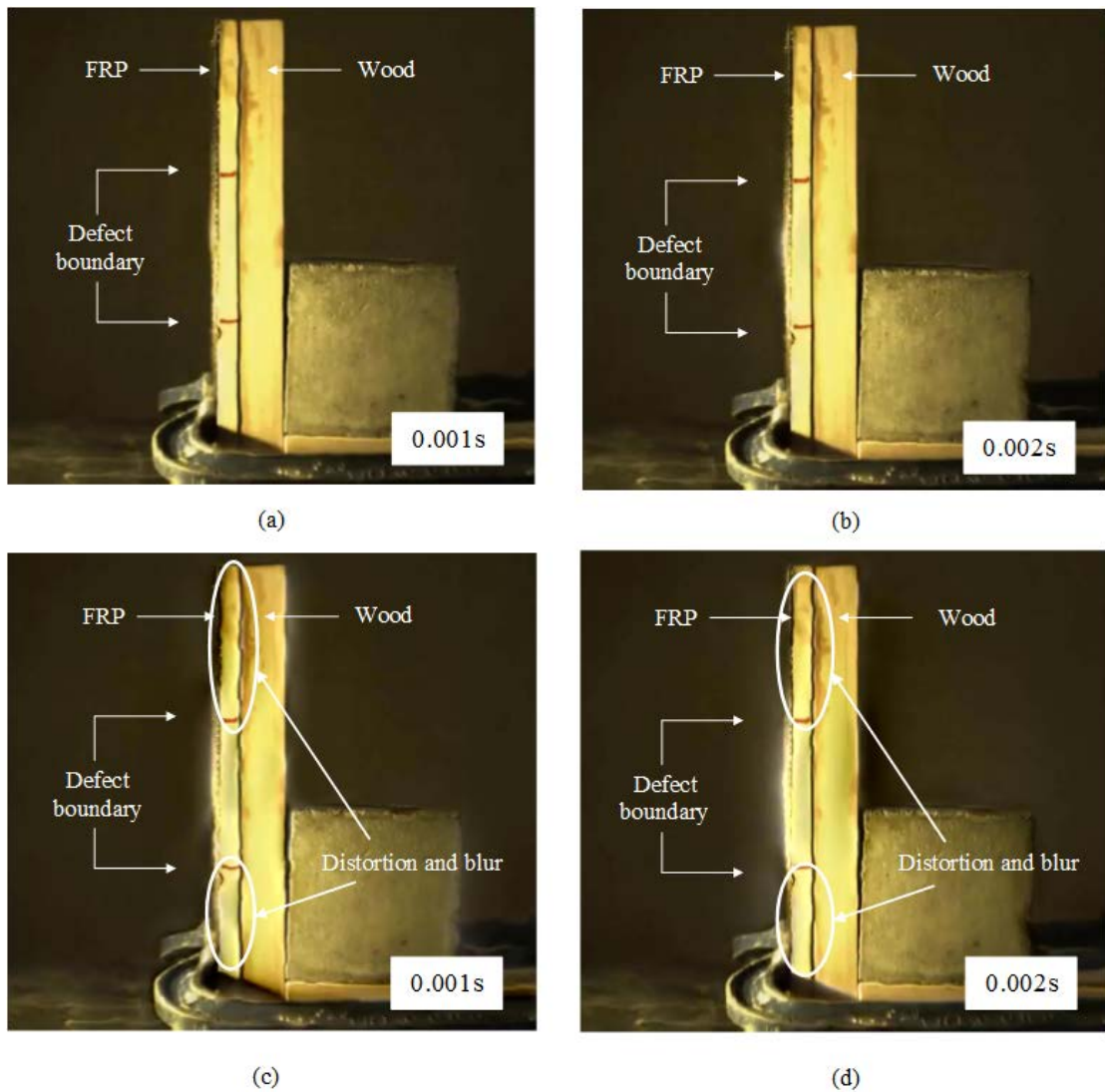


Figure 8. Images of vibrating FRP-bonded structural system with different motion amplification factors: amplification factor of 200 at (a) 0.001s and (b) 0.002s, and amplification factor of 5000 at (c) 0.001s and (d) 0.002s. Image distortion for FRP-bonded wood plate is found when amplification factor of 5000 is applied. Such high motion amplification factor can reduce the accuracy of defect detection by using this video processing technique.

In view of this concern, we have investigated the surface displacement at the defect centre under the motion amplification factor from 0 to 5000. The results from Figure 9 reveal that the surface displacement is linearly increased when the motion amplification factor is increased from 0 to 100. However, when the amplification factor exceeds 500 this trend is deviated significantly. This can be explained by Equation (14) that amplification factor α is too large, causing the equation invalid. With respect to the FRP-bonded structural system with defect area of $125 \text{ mm} \times 125 \text{ mm}$, the amplification factor between 50 and 500 can be considered as the suitable range for defect visualization as it can perform a sensitive motion magnification with little unwanted signal (noise). In this paper, methods and procedures for selecting of appropriate motion amplification factor for defect detection of FRP-bonded structural

system by using phase-based motion magnification technique is recommended in the next section.

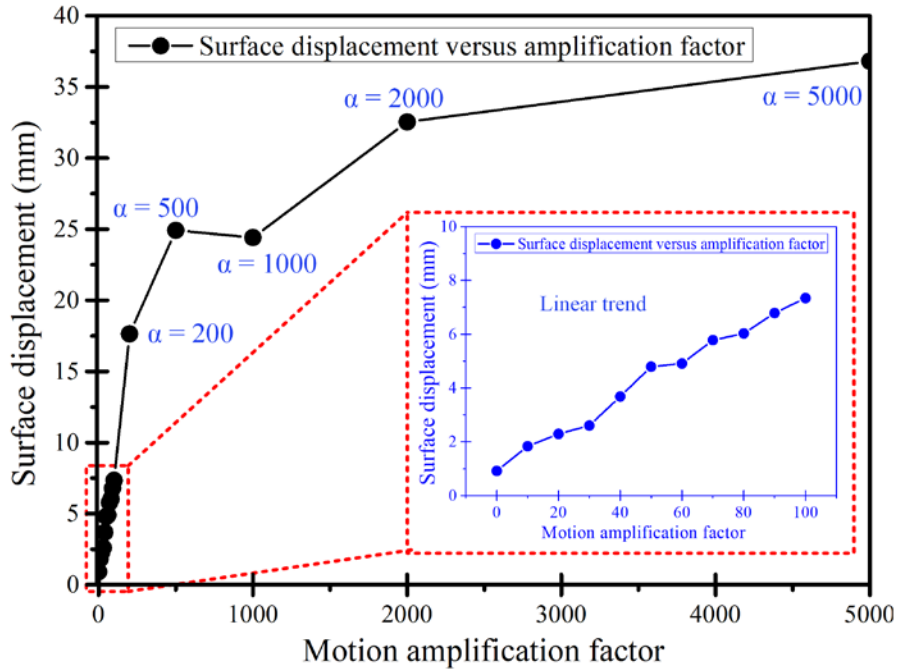


Figure 9. Surface displacement with bandpass frequency range of 0.25–0.50 Hz and with different motion amplification factors from 0 to 5000. Below amplification factor of 100, the linear trend of surface displacement is found. When the amplification factor exceeds 500, a large deviation can be resulted.

4.3. Effect of bandpass frequency range on defect detection

In this study, the frame rate used in the high speed camera is 1000 Hz and the output frame rate in the video is 1 Hz. Given the defect geometry and material properties of

FRP at the defect region, the natural frequency of surface vibration is approximately 450 Hz, as calculated by Equation (17). During the defect detection, the instant air pressure was applied at the central position of defect region. After excitation, the free vibration at its fundamental mode and natural frequency for the defect region is thought to occur. In this circumstance, the frequency of surface vibration in the video becomes 0.45 Hz. In view of Nyquist frequency principle, the bandpass frequency range that can be handled in the video processing is ranged from 0 and 0.5 Hz. In order to demonstrate the effect of bandpass frequency, the motion magnification is conducted with two frequency ranges: 0–0.25 Hz and 0.25–0.50 Hz, while the amplification factor is set as 100. From Figure 6, it can be found that the surface displacement magnified by frequency range of 0.25–0.50 Hz is much more significant than that magnified by frequency range of 0–0.25 Hz. The convex shape of displacement curve for the frequency range of 0.25–0.50 Hz is more remarkably shown. Since the vibration frequency (0.45 Hz) of FRP surface presented in video is included within the range of 0.25–0.50 Hz, the resonant vibration phenomenon could be stronger.

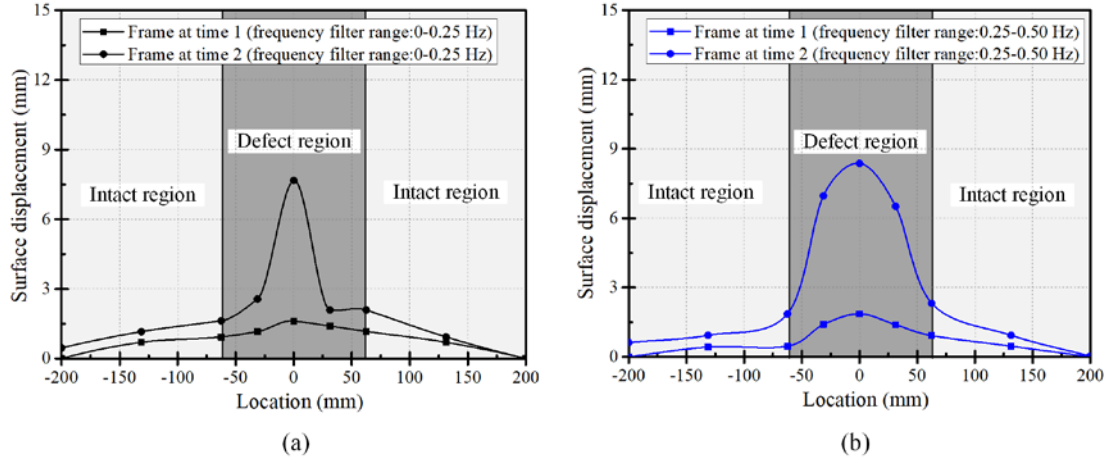


Figure 10. Motion magnification with amplification factor of 100 and with two different bandpass frequency ranges: (a) 0–0.25 Hz and (b) 0.25–0.50 Hz. Motion magnification with frequency filter range of 0.25–0.50 Hz results in more significant surface displacement than that with frequency filter range of 0–0.25 Hz. As the natural frequency of surface vibration presented in video is 0.45 Hz and this value falls in the range of 0.25–0.50 Hz, more significant resonant vibration is resulted.

In order to better evaluate the motion magnification performance based on the measurement points in Figure 10, the signal-to-noise ratio (SNR) is defined by dividing A_d (area under the shape curve for defect region) with A_i (area under the shape curve for intact region), as expressed by Equation (18).

$$SNR = \frac{A_d}{A_i} \quad (18)$$

It is clearly estimated from Figure 10 that SNR level for bandpass frequency range of 0.25–0.50 Hz is higher than that for frequency range of 0–0.25 Hz. This suggests that an appropriate selection of bandpass frequency range can sensitively magnify the structural motion without inducing much unwanted information. In the recommendation section, methods and procedures for selecting of appropriate bandpass frequency range for defect detection of FRP-bonded structural system by using phase-based motion magnification technique are discussed.

4.4. Discussion on defect detection of FRP-bonded structural system by phase-based motion magnification technique

In this research, the phase-based motion magnification has been demonstrated to be able to detect the interfacial defect in FRP-bonded wood structure. In fact, this video processing technique can be extended to other FRP-bonded structural systems such as FRP-bonded concrete and FRP-bonded steel structures. In addition, the phase-based motion magnification has the ability to evaluate the bonding condition of structures with coatings, such as wall element with thermal coating layer. The main contributions of this study are demonstrating a methodology for defect detection of FRP-bonded structural systems by using computer vision technique which supplements the existing detection techniques in structural inspection. This method

has the benefits over the traditional detection techniques towards FRP-bonded structural system in two aspects: (a) defect in structure can be visualized and observed directly in video recorded by high speed camera, without relying on the complicated interpretation of mechanical and electromagnetic signals, and (b) efficiency of defect detection is significantly improved since that setting up the test equipment is more convenient and detection is conducted by observing the processed video showing the whole structural surface instead of point-by-point measurement.

5. RECOMMENDATION AND FUTURE WORK

5.1. Recommendation of selecting appropriate motion amplification factor in detection

As previously mentioned, increasing the amplification factor can enlarge the surface motion for FRP-bonded structural system. This is the beneficial aspect for defect detection towards the structure since the interfacial defect region can be more easily observed. However, too large motion amplification factor can lead to the reduction in SNR ratio due to the initiation of flaws caused by the limited support of Gaussian window. Here, the suitable amplification factor for video processing can be determined by following the procedures as shown in Figure 11(a), which corresponds to the satisfactory SNR ratio. Motion magnification is performed with increasing

amplification factors, and the SNR ratios are calculated accordingly. When the SNR ratio reaches the desirable value, the corresponding amplification factor can be selected in the video processing.

5.2. Recommendation of selecting appropriate bandpass frequency range in detection

Besides the motion amplification factor, the selection of bandpass frequency range can be conducted by the following steps as shown in Figure 1(b). According to the output frame rate, the total bandpass frequency range is determined. Then, the motion magnification is performed with refining the bandpass frequency range, with the purpose to make the frequency range approach to the natural frequency of structural vibration. Similarly, when the SNR ratio reaches the desirable value, the corresponding bandpass frequency range is selected in the video processing.

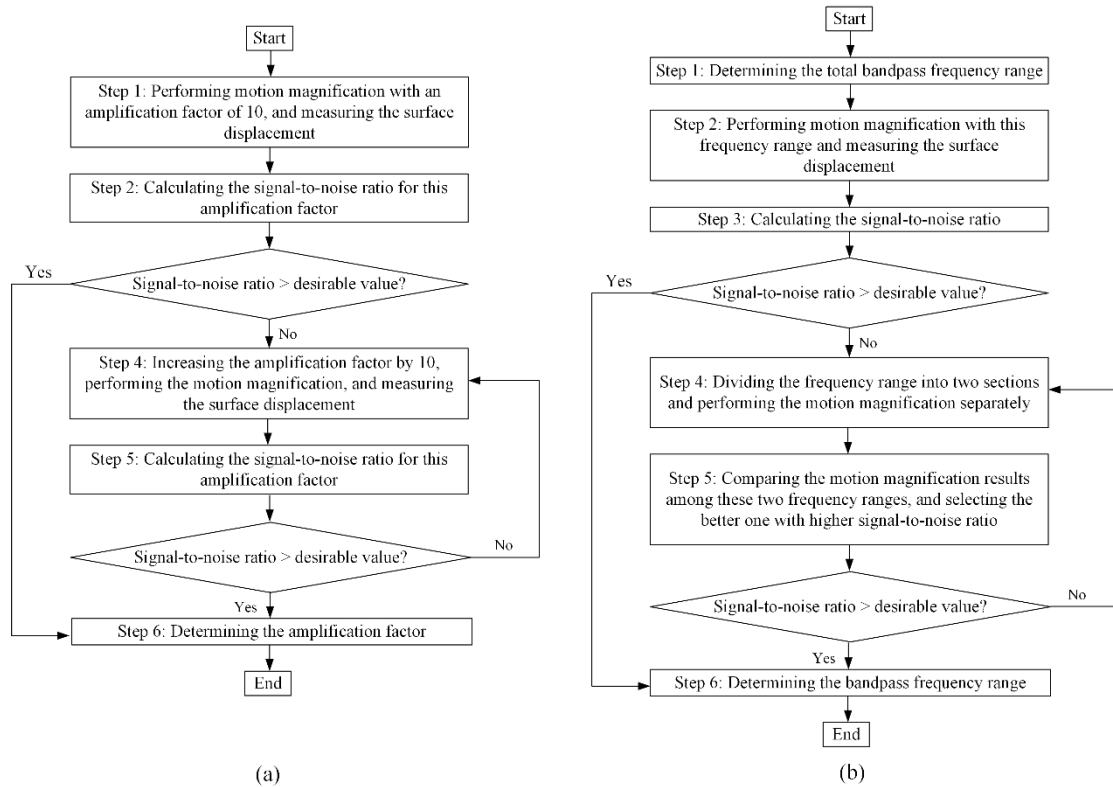


Figure 11. Procedures of selecting the appropriate (a) motion amplification factor and (b) bandpass frequency range in the phase-based motion magnification technique for defect detection of FRP-bonded structural system with satisfactory signal-to-noise ratio.

5.3. Future work

To further improve this methodology used in detecting FRP-bonded structural system, several research aspects are needed to be considered. In this experiment, the high speed camera was positioned laterally to clearly capture the mode shape of defect

region and measure its surface displacement with the purpose to achieve a more quantitative evaluation. In fact, the proposed technique is able to identify the presence of defect when the camera is positioned in the front of FRP-bonded system to record the FRP in-plane surface, as demonstrated by our previous conference paper [57]. Since that the use of a single camera can only obtain the in-plane motion information [40], it has limited capacity to precisely acquire the mode shape and out-of-plane surface displacement of defect region that is viewed in front position of structural element. To further improve the proposed technique in more realistic cases, the use of a stereo camera together with the three-dimensional digital image correlation method [58] will be beneficial for developing this detection scheme which allows for three-dimensional measurement of structural response at one position. In addition, algorithms that automatically extract the vibration amplitude at defect region in time series from the magnified video would be immensely useful for better characterizing of defect in bonded structural system. The time series vibration amplitude can be further transferred into the frequency spectrum so that the natural frequency of local defect region can be acquired. This natural frequency can be further taken to quantify the defect area of structure. In addition, the effect of defect size on the inspection results from this methodology is need to be investigated. Too small defect area can lead to large natural vibration frequency, which requires higher

frame rate of camera recording. It is necessary to figure out the minimum defect size detected by this video processing technique and its relation to the capacity of high speed camera. Furthermore, modal analysis (*e.g.* measurement of the quantitative two dimensional deflection shapes) from the magnified video benefits the understanding of dynamic properties of the FRP-bonded structural system.

6. CONCLUSION

The results of an experimental study to investigate the ability of phase-based motion magnification video processing technique to detect interfacial defect between FRP composite and basis material are presented in this paper. Research findings demonstrate that under an instant air blow the surface motion at the defect region of FRP-bonded structural system is hard to be perceived without applying the motion magnification technique. However, the motion behaviour at the defect region can be clearly distinguished from the intact region when adopting this methodology, justifying the effectiveness of phase-based motion magnification for defect detection in FRP-bonded structural systems. Our investigation also indicates that the appropriate selection of bandpass frequency range is critical to the detection accuracy of structural system. When the filtered frequency range covers the natural frequency of structural vibration, the motion can be magnified more efficiently and effectively.

Besides, the motion amplification factor should be selected carefully during the video processing. Too large motion amplification factor can lead to image distortion and can result in an inaccurate detection. In this paper, recommendations are provided for selecting the appropriate bandpass frequency range and motion amplification factor for the video processing technique when it is applied in defect detection of FRP-bonded structural systems.

ACKNOWLEDGEMENTS

The authors are grateful to the financial support from Croucher Foundation through the Start-up Allowance for Croucher Scholars (No. 9500012). The support from the Research Grants Council (RGC) in Hong Kong through the Early Career Scheme (ECS) (No. 139113) is also gratefully acknowledged.

REFERENCES

- [1] Zhao X, Zhang L. State-of-the-art review on FRP strengthened steel structures. *Engineering Structures* 2007; **29**(8): 1808-1823.
- [2] Tam L-h, Zhou A, Yu Z, Qiu Q, Lau D. Understanding the effect of temperature on the interfacial behavior of CFRP-wood composite via molecular dynamics simulations. *Composites Part B: Engineering* 2017; **109**: 227-237.

- [3] Kalfat R, Al-Mahaidi R. Improvement of FRP-to-concrete bond performance using bidirectional fiber patch anchors combined with FRP spike anchors. *Composite Structures* 2016; **155**: 89-98.
- [4] Strauss A, Pascale G, Bonfiglioli B, Bergmeister K, Muro PD. Probability and sensitivity analysis of strain measurements in FRP. *Structural Control and Health Monitoring* 2004; **11**(4): 55-74.
- [5] Gustavsson L, Sathre R. Variability in energy and carbon dioxide balances of wood and concrete building materials. *Building and Environment* 2006; **41**(7): 940-951.
- [6] Natterer JK. New technologies for engineered timber structures. *Progress in Structural Engineering and Materials* 2002; **4**(3): 245-263.
- [7] Jesus AMPd, Pinto JMT, Morais JLL. Analysis of solid wood beams strengthened with CFRP laminates of distinct lengths. *Construction and Building Materials* 2012; **35**: 817-828.
- [8] Lau D, Qiu Q, Zhou A, Chow CL. Long term performance and fire safety aspect of FRP composites used in building structures. *Construction and Building Materials* 2016; **126**: 573-585.
- [9] Riley R, Salamov AA, Brown DW, Nagy LG, Floudas D, Held BW, Levasseur A, Lombard V, Morin E, Otilar R, Lindquist EA, Sun H, LaButti KM, Schmutz J,

- Jabbour D, Luo H, Baker SE, Pisabarro AG, Walton JD, Blanchette RA, Henrissat B, Martin F, Cullen D, Hibbett DS, Grigoriev IV. Extensive sampling of basidiomycete genomes demonstrates inadequacy of the white-rot/brown-rot paradigm for wood decay fungi. *Proceedings of the National Academy of Sciences of the United States of America* 2014; **111**(27): 9923-9928.
- [10]Severo ETD, Calonego FW, Sansígolo CA, Bond B. Changes in the chemical composition and decay resistance of thermally-modified hevea brasiliensis wood. *PLoS ONE* 2016; **11**(3): 1-10.
- [11]Skyba O, Douglas CJ, Mansfield SD. Syringyl-rich lignin renders poplars more resistant to degradation by wood decay fungi. *Applied and environmental microbiology* 2013; **79**(8): 2560 -2571.
- [12]Sandak A, Sandak J, Riggio M. Assessment of wood structural members degradation by means of infrared spectroscopy: an overview. *Structural Control and Health Monitoring* 2016; **23**(3): 396-408
- [13]Qin R, Qiu Q, Lam JHM, Tang AMC, Leung MWK, Lau D. Health assessment of tree trunk by using acoustic-laser technique and sonic tomography. *Wood Science and Technology* 2018: in press.
- [14]Lau D, Qiu Q. A review of nondestructive testing approach using mechanical and electromagnetic waves. *Proc. SPIE 9804, Nondestructive Characterization and*

Monitoring of Advanced Materials, Aerospace, and Civil Infrastructure Las Vegas, United States, 2016.

- [15] Wang L, Liu Y, Fu W, Li F, Zhao Z, Yu K. Source location using an optimized microfiber coupler sensor based on modal acoustic emission method. *Structural Control and Health Monitoring* 2017: in press.
- [16] Abouhussien AA, Hassan AAA. Acoustic emission-based analysis of bond behavior of corroded reinforcement in existing concrete structures. *Structural Control and Health Monitoring* 2016; **24**(3): e1893.
- [17] Cheng TK, Lau D. A photophone-based remote NDT approach to interfacial defect detection in FRP-bonded systems. *Structural Health Monitoring* 2017; **17**(2): 135-144.
- [18] Scarponi C, Briotti G. Ultrasonic technique for the evaluation of delaminations on CFRP, GFRP, KFRP composite materials. *Composites Part B: Engineering* 2000; **31**(3): 237--243.
- [19] Yu T-Y, Büyüköztürk O. A far-field airborne radar NDT technique for detecting debonding in GFRP-retrofitted concrete structures. *NDT & E international* 2008; **41**: 10-24.

- [20] Büyüköztürk O, Yu T-Y. Far-field radar NDT technique for detecting GFRP debonding from concrete. *Construction and Building Materials* 2009; **23**: 1678-1689.
- [21] Brown JR, Hamilton HR. Quantitative infrared thermography inspection for FRP applied to concrete using single pixel analysis. *Construction and Building Materials* 2013; **38**: 1292-1302.
- [22] Tashan J, Al-Mahaidi R. Bond defect detection using PTT IRT in concrete structures strengthened with different CFRP systems. *Composite Structures* 2014; **114**: 13-19.
- [23] Sun R, Sevillano E, Perera R. Debonding detection of FRP strengthened concrete beams by using impedance measurements and an ensemble PSO adaptive spectral model. *Composite Structures* 2015; **125**: 374-387.
- [24] Qiu Q, Lau D. Use of laser reflection technique for defect detection in CFRP concrete systems. Proc. SPIE 9804, Nondestructive Characterization and Monitoring of Advanced Materials, Aerospace, and Civil Infrastructure. Las Vegas, United States, 2016.
- [25] Qiu Q, Lau D. A novel approach for near-surface defect detection in FRP-bonded concrete systems using laser reflection and acoustic-laser techniques. *Construction and Building Materials* 2017; **141**: 553-564.

- [26] Qiu Q, Lau D. Experimental evaluation on the effectiveness of acoustic-laser technique towards the FRP-bonded concrete system. *Proc. SPIE 9437, Structural Health Monitoring and Inspection of Advanced Materials, Aerospace, and Civil Infrastructure*, 2015.
- [27] Qiu Q, Lau D. The sensitivity of acoustic-laser technique for detecting the defects in CFRP-bonded concrete systems. *Journal of Nondestructive Evaluation* 2016; **35**: 1-10.
- [28] Yu T, Cheng TK, Zhou A, Lau D. Remote defect detection of FRP-bonded concrete system using acoustic-laser and imaging radar techniques. *Construction and Building Materials* 2016; **105**: 146-155.
- [29] Cha Y-J, Choi W, Büyüköztürk O. Deep learning-based crack damage detection using convolutional neural networks. *Computer-Aided Civil and Infrastructure Engineering* 2017; **32**(5): 361-378.
- [30] Qiu Q, Lau D. Measurement of structural vibration by using optic-electronic sensor. *Measurement* 2018; **117**: 435-443.
- [31] Taillade F, Quiertant M, Benzarti K, Aubagnac C. Shearography and pulsed stimulated infrared thermography applied to a nondestructive evaluation of FRP strengthening systems bonded on concrete structures. *Construction and Building Materials* 2011; **25**: 568-574.

- [32] Angelis GD, Meo M, Almond DP, Pickering SG, Angioni SL. A new technique to detect defect size and depth in composite structures using digital shearography and unconstrained optimization. *NDT & E International* 2012; **45**: 91-96.
- [33] Cha Y-J, Choi W, Vision-based concrete crack detection using a convolutional neural network. In *Conference Proceedings of the Society for Experimental Mechanics Series*, Springer, Cham: 2017.
- [34] Chen JG, Davis A, Wadhwa N, Durand F. Video camera-based vibration measurement for civil infrastructure applications. *Journal of Infrastructure Systems* 2017; **23**(3): B4016013.
- [35] Chen Z, Li H, Bao Y, Li N, Jin Y. Identification of spatio-temporal distribution of vehicle loads on long-span bridges using computer vision technology. *Structural Control and Health Monitoring* 2015; **11**(1): 517-534.
- [36] Tung Khuc, Catbas FN. Completely contactless structural health monitoring of real-life structures using cameras and computer vision. *Structural Control and Health Monitoring* 2017; **24**(1): e1852
- [37] Durand F, Freeman WT, Rubinstein M. A world of movement. *Sci.Am.* 2015; **312**(1): 46-51.
- [38] Wadhwa N, Rubinstein M, Durand F, Freeman WT. Phase-based video motion processing. *ACM Transactions on Graphics* 2013; **32**(4).

- [39]N. Wadhwa, M. Rubinstein, F. Durand, W.T. Freeman, Riesz pyramids for fast phase-based video magnification, in: 2014 IEEE International Conference on Computational Photography (ICCP), 2014.
- [40]Chen JG, Wadhwa N, Cha Y-J, Durand F, Freeman WT, Buyukozturk O. Modal identification of simple structures with high-speed video using motion magnification. *Journal of Sound and Vibration* 2015; **345**: 58-71.
- [41]Fleet DJ, Jepson AD. Computation of component image velocity from local phase information. *International journal of computer vision* 1990; **5**: 77-104.
- [42]Gautama T, Hulle MAV. A phase-based approach to the estimation of the optical flow field using spatial filtering. *IEEE Transactions on Neural Networks* 2002; **13**(5): 1127 - 1136.
- [43]Fuchs M, Chen T, Wang O, Raskar R, Seidel H-P, Lensch HPA. Real-time temporal shaping of high-speed video streams. *Computers & Graphics* 2010; **34**(5): 575-584.
- [44]Luz EJdS, Menotti D, Schwartz WR. Evaluating the use of ECG signal in low frequencies as a biometry. *Expert Systems with Applications* 2014; **41**(5): 2309-2315.

- [45] Wadhwa N, Wu H-Y, Davis A, Rubinstein M, Shih E, Mysore GJ, Chen JG, Buyukozturk O, Gutttag JV, Freeman WT, Durand F. Eulerian video magnification and analysis. *Communications of the ACM* 2017; **60**: 87-95.
- [46] Sarrafi A, Mao Z. Uncertainty quantification of phase-based motion estimation on noisy sequence of images. *Proc. SPIE 10170, Health Monitoring of Structural and Biological Systems, 2017* 2017.
- [47] Cha Y-J, Chen JG, Büyüköztürk O. Output-only computer vision based damage detection using phase-based optical flow and unscented Kalman filters. *Engineering Structures* 2017; **132**: 300-313.
- [48] Sarrafi A, Poozesh P, Niezrecki C, Mao Z. Mode extraction on wind turbine blades via phase-based video motion estimation. *Proc. SPIE 10171, Smart Materials and Nondestructive Evaluation for Energy Systems, 2017* 2017.
- [49] D. Lau, One dimensional predictive model of interfacial stiffness in FRPbonded concrete system using acoustic-laser technique, in: *Proc. SPIE 8694, Nondestructive Characterization for Composite Materials, Aerospace Engineering, Civil Infrastructure, and Homeland Security, 2013*.
- [50] W. Soedel. *Vibrations of Shells and Plates, Third Edition*. Boca Raton, United States: CRC Press; 2004.

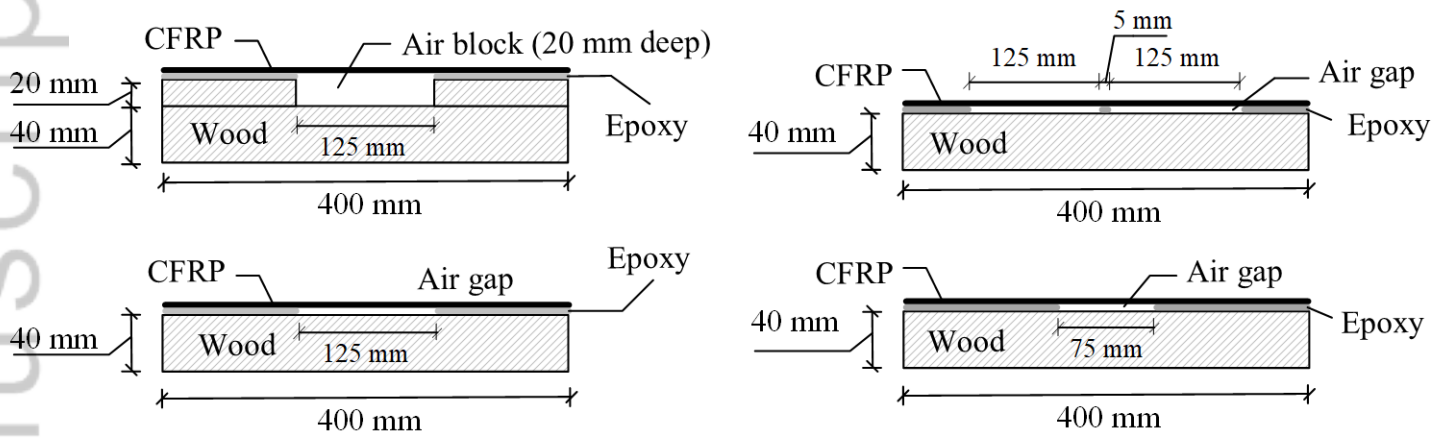
- [51]T.K. Cheng, D. Lau. Vibrational characteristics of FRP-bonded concrete interfacial defects in a low frequency regime. Proc. SPIE 9063, Nondestructive Characterization for Composite Materials, Aerospace Engineering, Civil Infrastructure, and Homeland Security, 2014.
- [52]Reddy JN, *Theory and Analysis of Elastic Plates and Shells*. second ed.; CRC press: 2006.
- [53]Lowa KH, Chaia GB, Lima TM, Suea SC. Comparisons of experimental and theoretical frequencies for rectangular plates with various boundary conditions and added masses. *International Journal of Mechanical Sciences* 1998; **40**(11): 1119-1131.
- [54]Dhotarad MS, Ganesan N. Vibration analysis of a rectangular plate subjected to a thermal gradient. *Journal of Sound and Vibration* 1978; **60**(4): 481-497.
- [55]Leissa AW. The free vibration of rectangular plates. *Journal of Sound and Vibration* 1973; **31**(3): 257-293.
- [56]Ramazani A, Ebrahimi Z, Prah U. Study the effect of martensite banding on the failure initiation in dual-phase steel. *Computational Materials Science* 2014; **87**: 241-247.
- [57]Qiu Q, Lau D In *Defect visualization in FRP-bonded concrete by using high speed camera and motion magnification technique*, Proc. SPIE 10169,

Nondestructive Characterization and Monitoring of Advanced Materials,
Aerospace, and Civil Infrastructure, Portland, Oregon, United States, 2017.

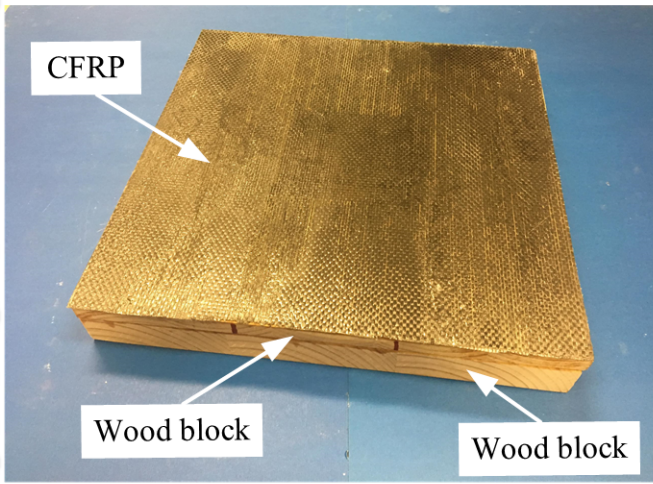
- [58] Helfrick MN, Niezrecki C, Avitabile P, Schmidt T. 3D digital image correlation methods for full-field vibration measurement. *Mechanical Systems and Signal Processing* 2011; **25**(3): 917-927.

Table 1 The smallest detectable dimension of defect in CFRP-bonded system with variation of maximum frame rate of commercially available high speed camera.

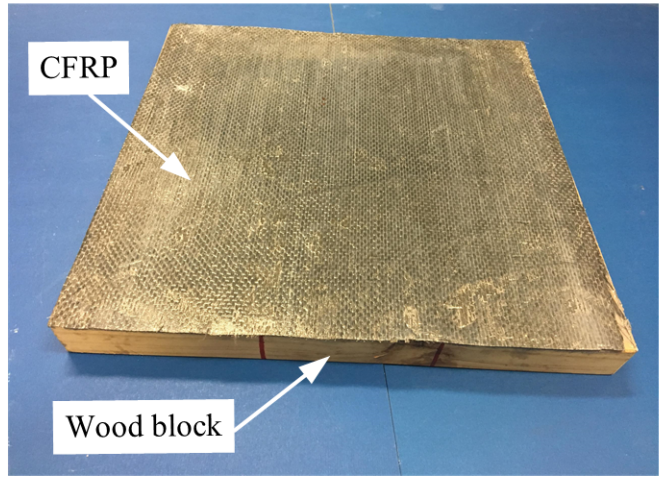
Maximum frame rate	Smallest detectable dimension
1000	120 mm × 120 mm
2000	84 mm × 84 mm
5000	53 mm × 53 mm
10000	37 mm × 37 mm
25000	24 mm × 24 mm



(a)



FRP-bonded wood with internal air block

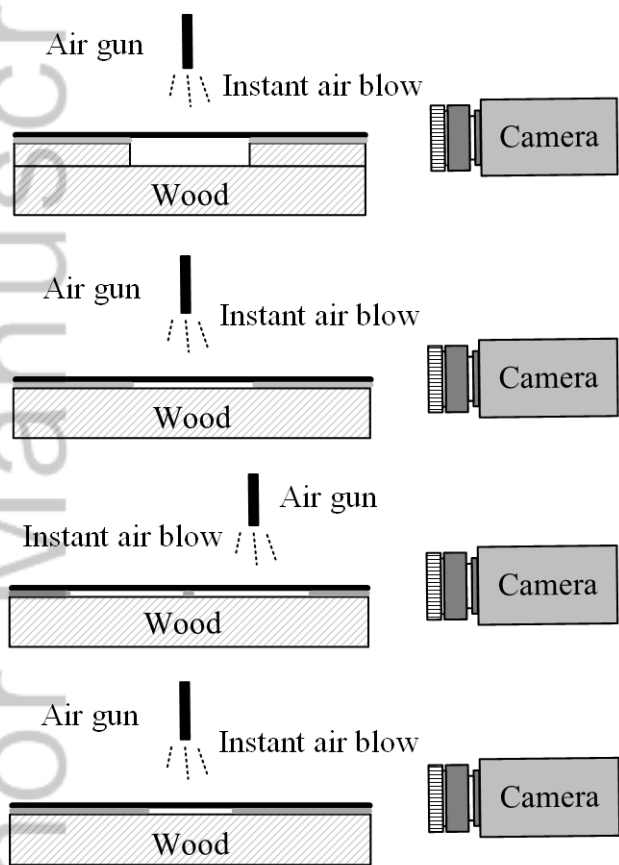


FRP-bonded wood with interfacial air gap

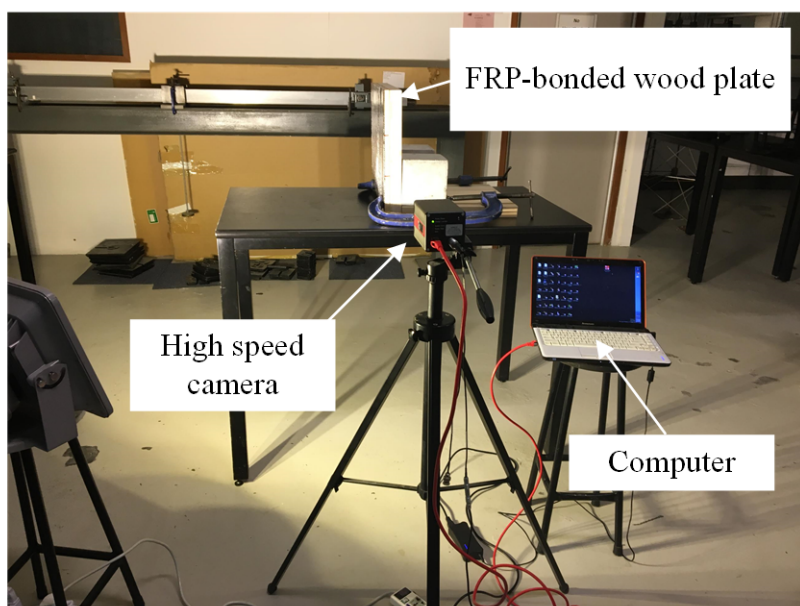
(b)

STC_2259_F1.tif

Author Manuscript

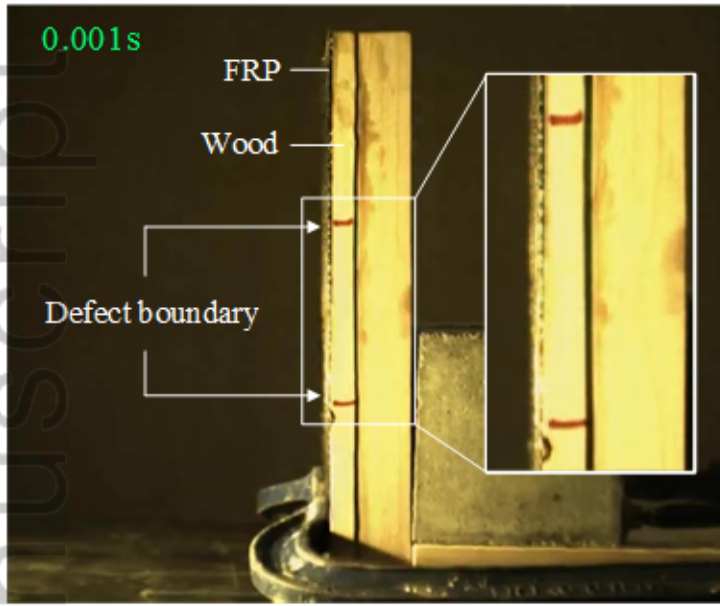


(a)

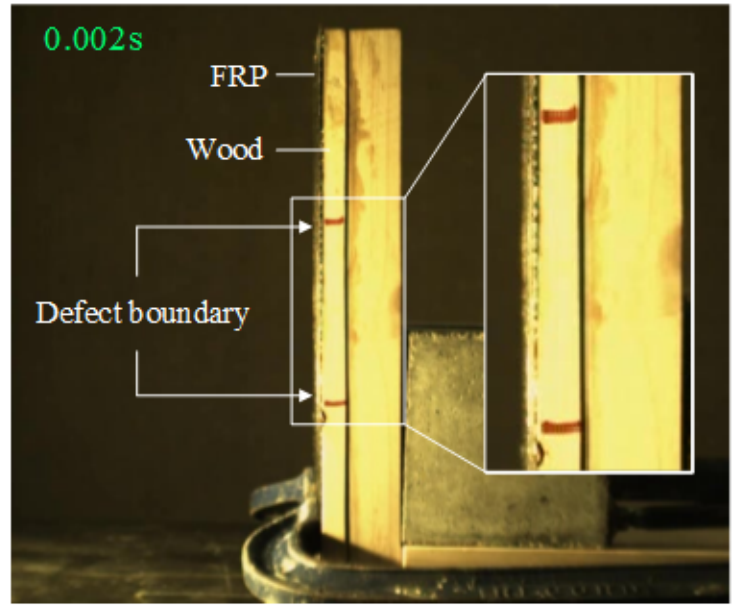


(b)

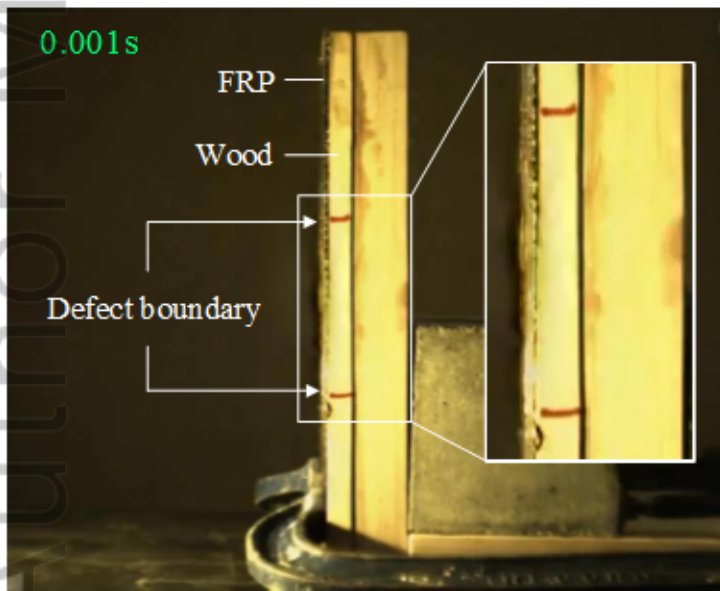
STC_2259_F2.tif



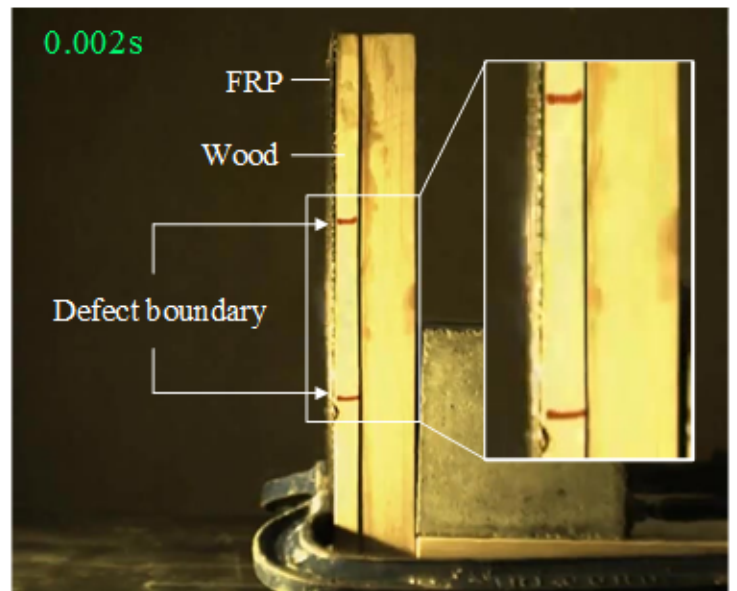
(a)



(b)

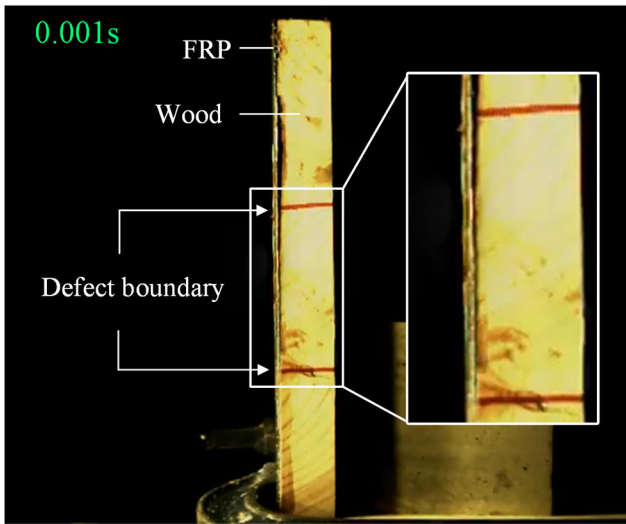


(c)

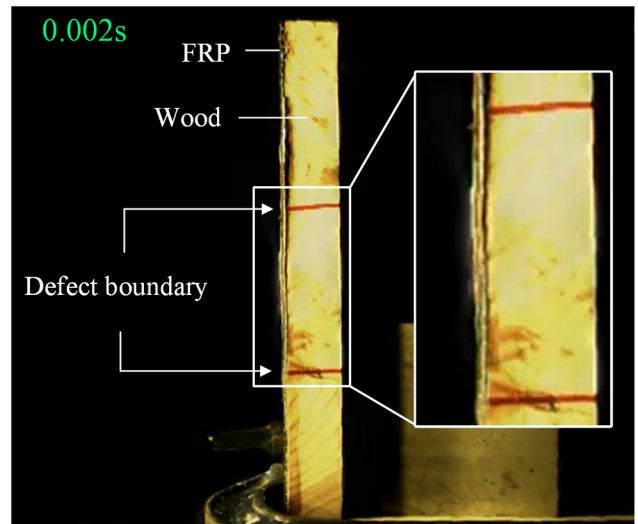


(d)

STC_2259_F3.tif

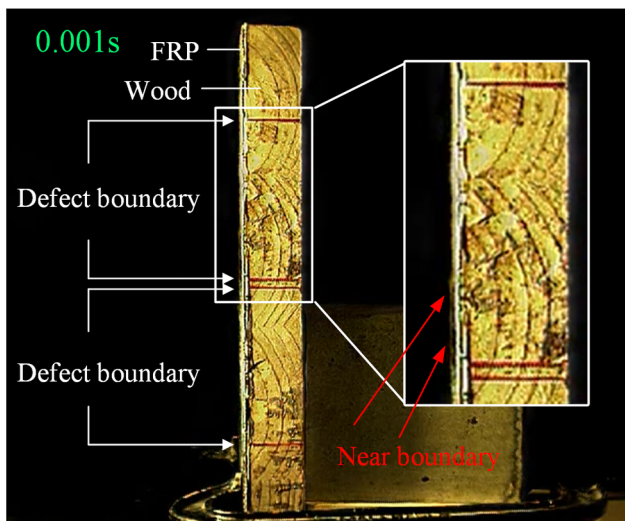


(a)

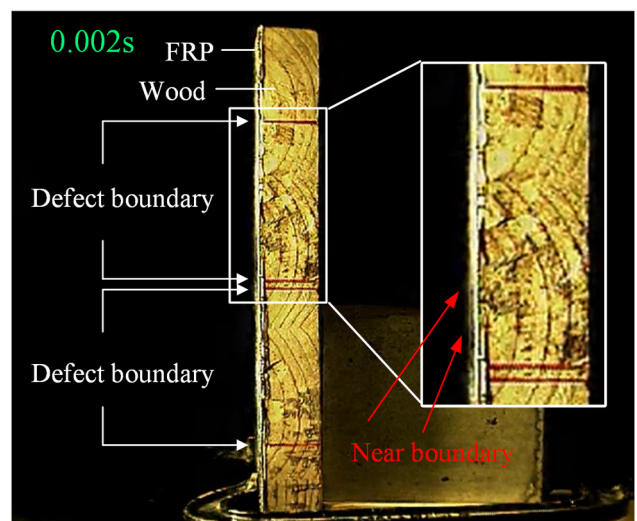


(b)

STC_2259_F4.tif

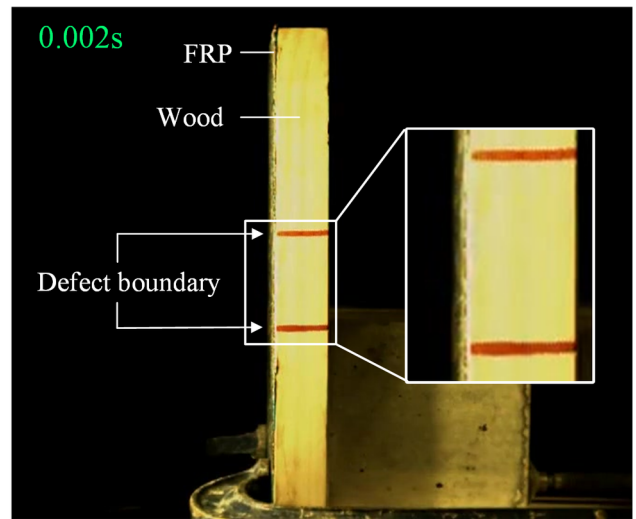
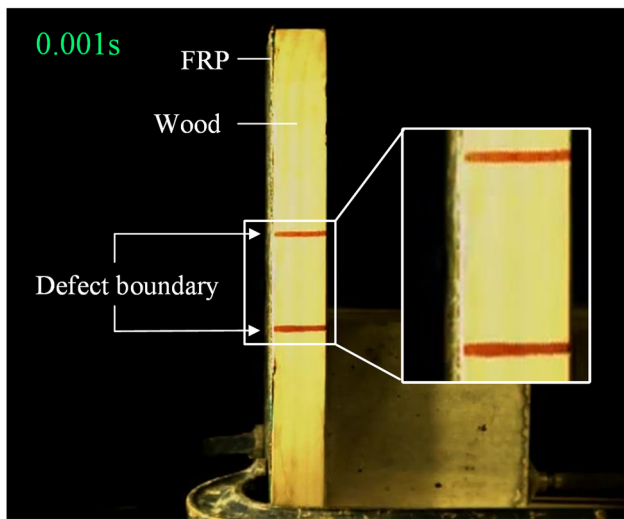


(a)

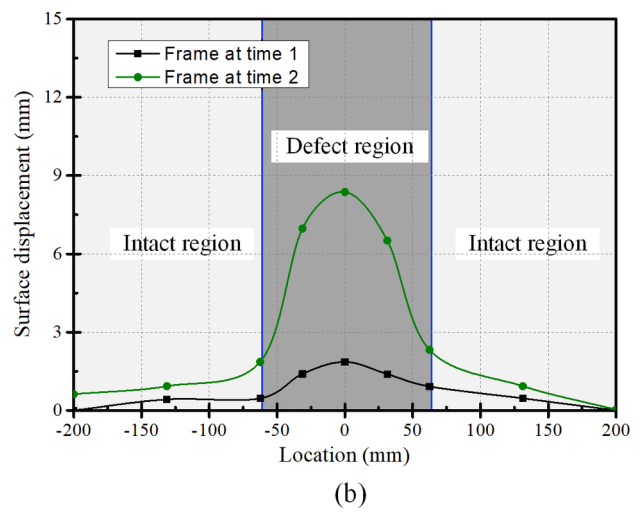
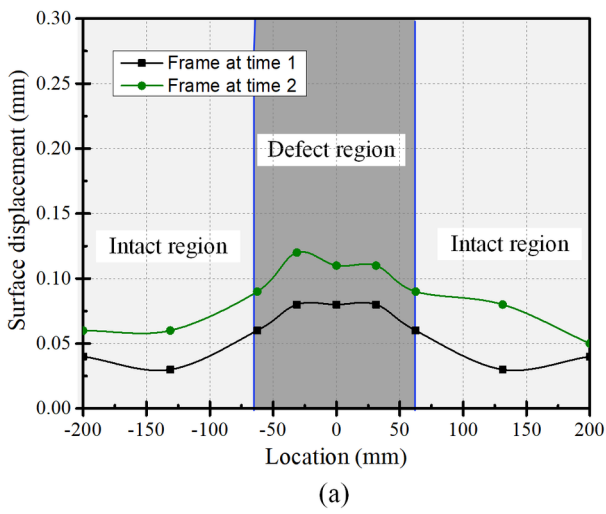


(b)

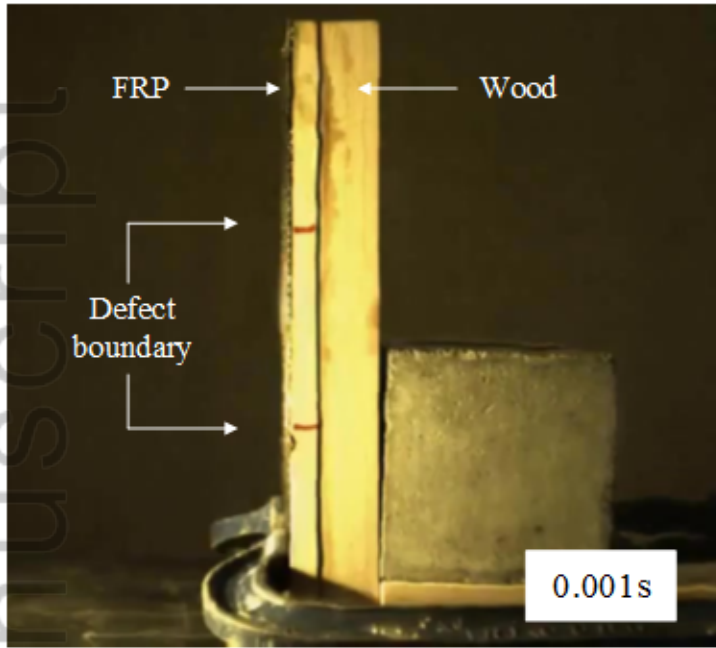
STC_2259_F5.tif



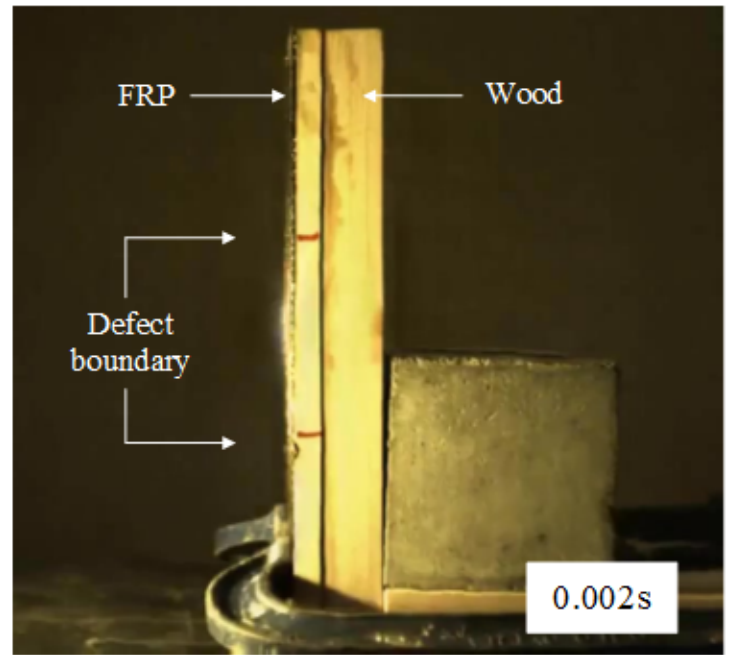
STC_2259_F6.tif



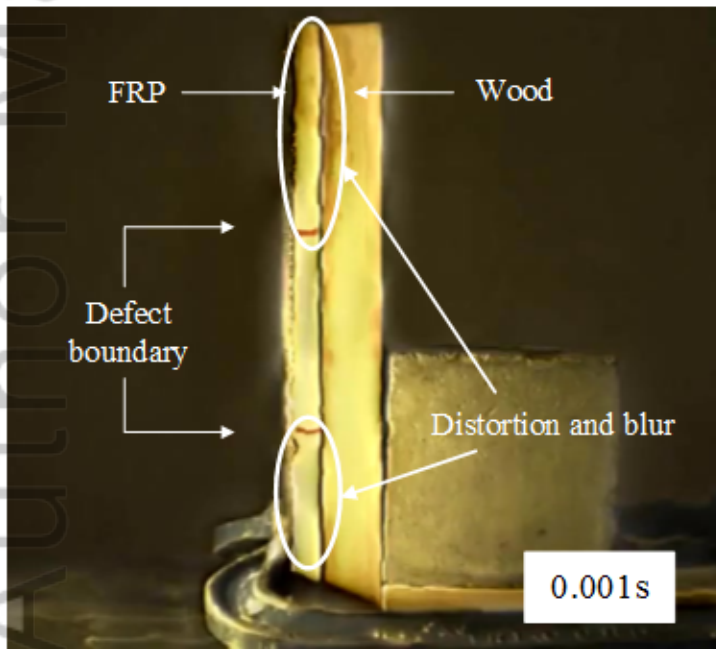
STC_2259_F7.tif



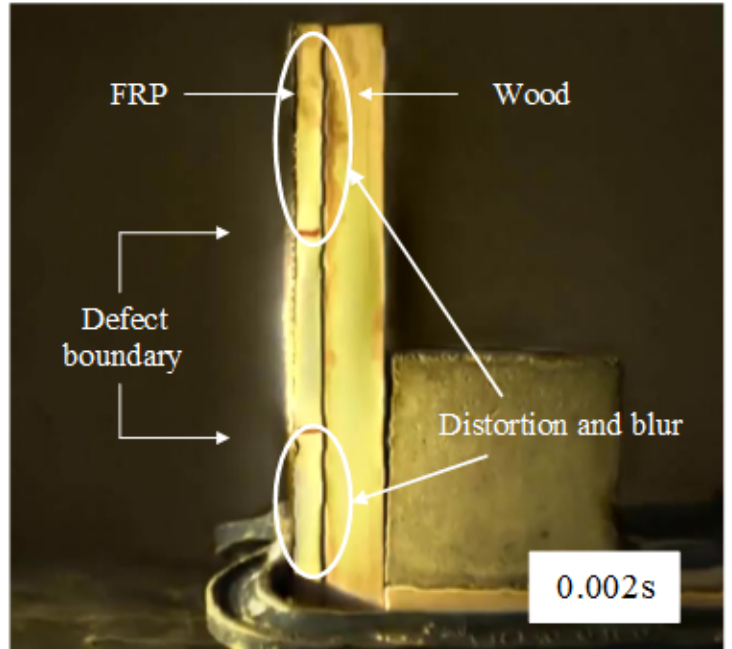
(a)



(b)

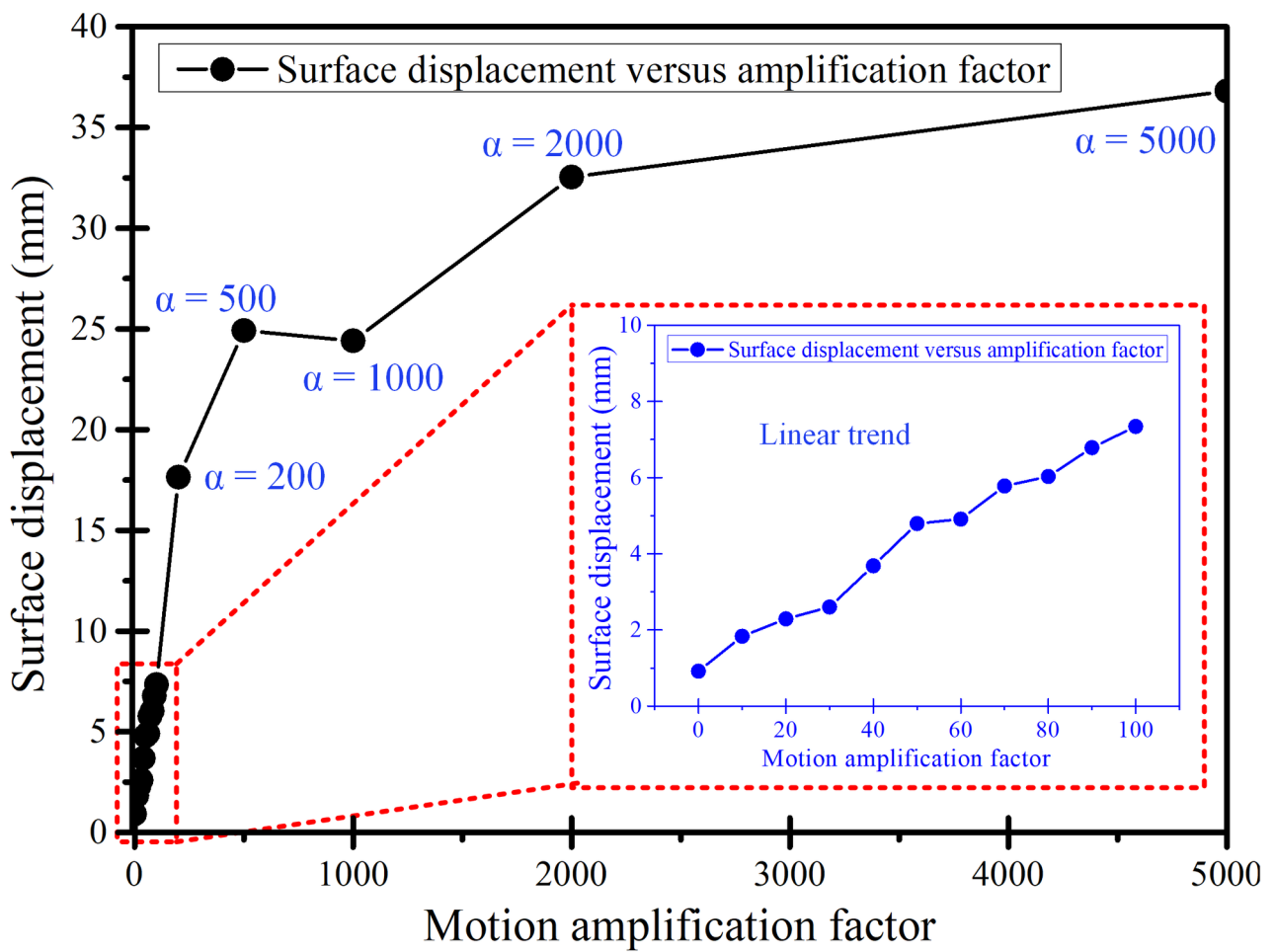


(c)

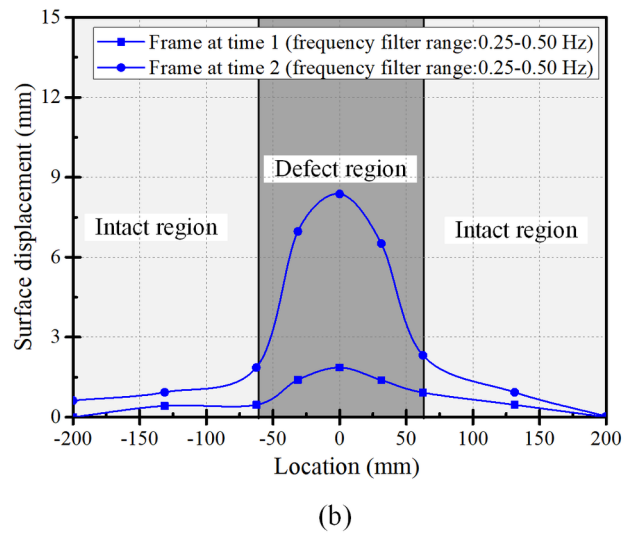
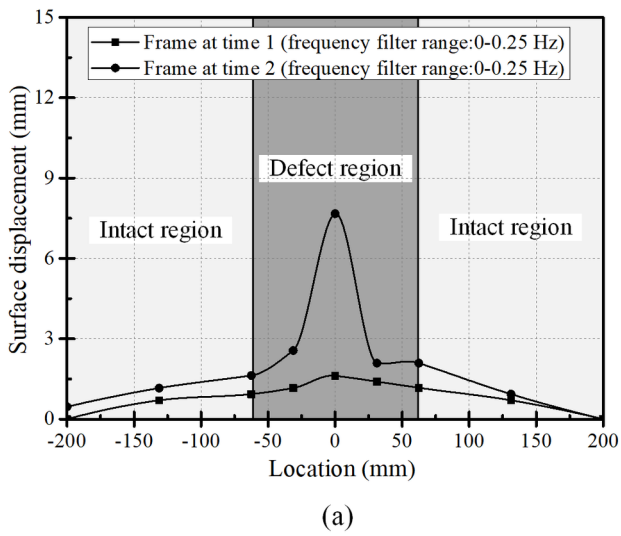


(d)

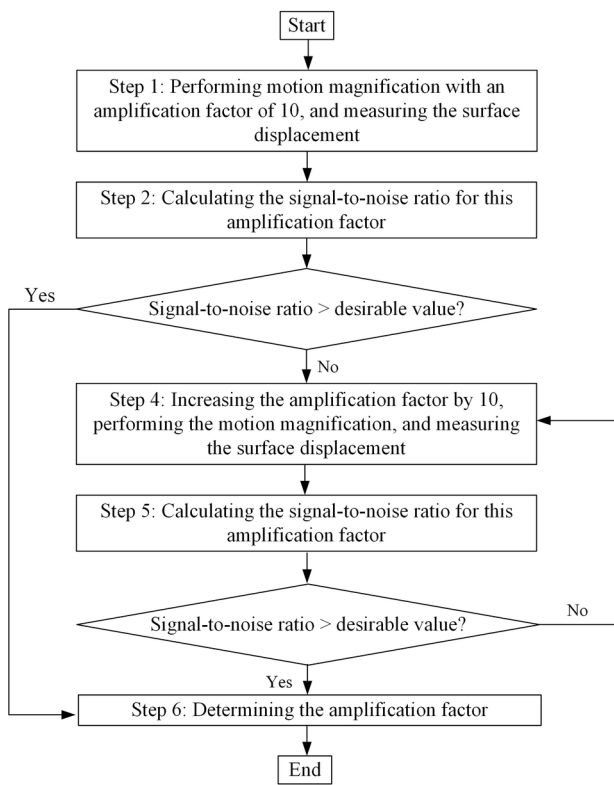
STC_2259_F8.tif



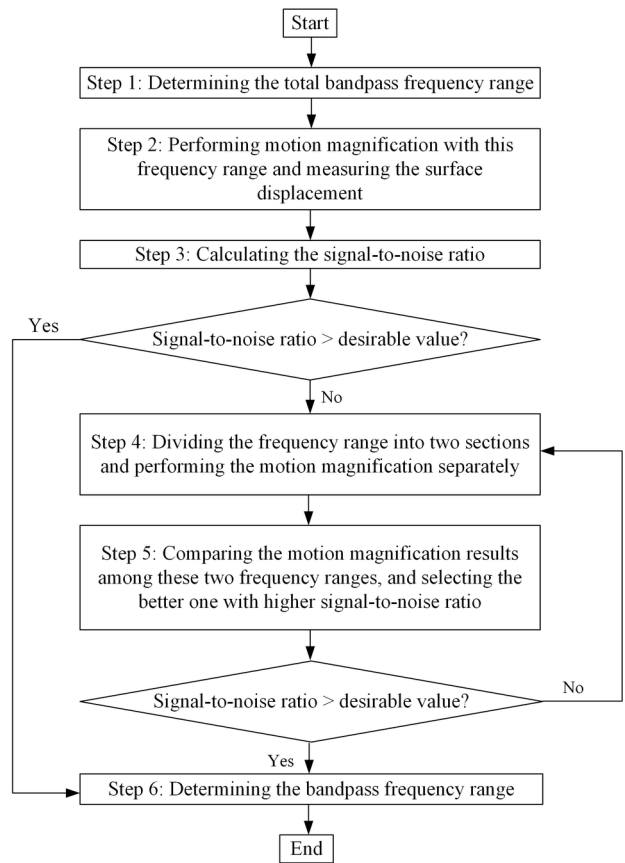
STC_2259_F9.tif



STC_2259_F10.tif



(a)



(b)

STC_2259_F11.tif